HIGH ACCURACY *AB INITIO* METHODS APPLIED TO PHOSPHAETHYNE AND PERCHLOROSILYLCARBENE

by

JUSTIN BOONE INGELS

(Under the Direction of Henry F. Schaefer)

ABSTRACT

High-accuracy *ab initio* methods have been applied to two chemical systems: phosphaethyne (HCP) and perchlorosilylcarbene (Cl-C-$SiCl_3$). HCP and its isomerization species linear HPC (found to be a second-order saddle point) have been characterized at couple cluster levels with triple contributions [CCSD(T), CCSDT-3, CC3] and a large correlation consistent basis set, cc-pV5Z. Eight singlet excited states were examined and characterized using the equation-of-motion coupled cluster method. For perchlorosilylcarbene, the potential energy surface was determined by optimizing three stationary points on both the singlet and triplet surfaces, including a focal-point analysis to nail down the relative energy differences. The infrared spectrum was predicted for each minima to help in determining the nature of the species trapped by Schreiner, *et. al.* The global minimum and the best fit for the infrared spectrum was the triplet carbene species, in line with previous experimental and theoretical work on analogous systems.

INDEX WORDS: computational chemistry, phosphaethyne, HCP, isophosphaethyne, HPC, coupled cluster, MP2, excited states, EOM, perchlorosilylcarbene, carbenes, focal-point

HIGH ACCURACY *AB INITO* METHODS APPLIED TO PHOSPHAETHYNE AND PERCHLOROSILYLCARBENE

by

JUSTIN BOONE INGELS

B.S., Northwest Missouri State University, 2004

A Thesis Submitted to the Graduate Faculty of The University of Georgia in Partial Fulfillment of the Requirements for the Degree

MASTER OF SCIENCE

ATHENS, GEORGIA

2007

HIGH ACCURACY *AB INITIO* METHODS APPLIED TO PHOSPHAETHYNE AND PERCHLOROSILYLCARBENE

by

JUSTIN BOONE INGELS

Major Professor: Henry F. Schaefer III

Committee: Nigel G. Adams
Geoffrey D. Smith

Electronic Version Approved:

Maureen Grasso
Dean of the Graduate School
The University of Georgia
May 2007

DEDICATION

I dedicate this work to my parents for their love and dedication to my life, even if from 900 miles away.

TABLE OF CONTENTS

CHAPTER 1

INTRODUCTION AND LITERATURE REVIEW

The stationary points on the ground and excited potential energy surfaces of HCP and the ground state surface of perchlorosilylcarbene have been systematically investigated using *ab initio* molecular electronic structure theory. For ground state stationary points, geometries have been optimized and physical properties predicted utilizing restricted self-consistent field theory, coupled cluster theory with single and double excitations (CCSD), CCSD with perturbative triple corrections [CCSD(T)], and/or CCSD with partial iterative triple excitations (CCSDT-3 and CC3). Linear HPC, a stationary point of Hessian index 2, is predicted to lie 75.2 kcal mol^{-1} above the global minimum HCP. The dissociation energy D_0 $\left[HCP\left(\widetilde{X}\ ^1\Sigma^+\right)\rightarrow\ H\left(^2S\right)+CP\left(X\ ^2\Sigma^+\right)\right]$ of HCP is predicted to be 119.0 kcal mol^{-1}, which is very close to the experimental lower limit of 119.1 kcal mol^{-1}. Eight singlet excited states were examined and their physical properties were determined employing three equation-of-motion coupled cluster methods (EOM-CCSD, EOM-CCSDT-3, and EOM-CC3). Four stationary points were located on the lowest-lying excited state potential energy surface, $^1\Sigma^-\rightarrow{}^1A''$, with excitation energies T_e of 101.4 kcal mol^{-1} $\left(^1A''\ HCP\right)$, 104.6 kcal mol^{-1} $\left(^1\Sigma^-\ HCP\right)$, 122.3 kcal mol^{-1} $\left(^1A''\ HPC\right)$, and 171.6 kcal mol^{-1} $\left(^1\Sigma^-\ HPC\right)$ at the cc-pVQZ EOM-CCSDT-3 level of theory. Perchlorosilylcarbene identified experimentally based on the IR spectrum and ESR signal of the molecule taken in the matrix. Focal-point extrapolations at the aforementioned levels of theory were utilized to definitively determine whether the trapped species is a singlet or triplet species. Our results show the triplet to be lower in energy than the singlet with regards to the perchlorosilylcarbene species. A vibrational analysis that includes anharmonic effects provides a means to compare to the IR spectra obtained experimentally. It was also found that the species formed upon isomerization, perchlorosilylethylene is less stable than the perchlorosilylcarbene species.

CHAPTER 2

CHARACTERIZATION OF SINGLET GROUND AND LOW-LYING ELECTRONIC EXCITED STATES OF PHOSPHAETHYNE AND ISOPHOSPHAETHYNE[1]

[1] J. B. Ingels, J. M. Turney, N. A. Richardson, Y. Yamaguchi, and H. F. Schaefer III, *J. Chem. Phys.* **125**, 104306 (2006). Reprinted here with permission of publisher.

2.1 Abstract

The singlet ground $\left(\widetilde{X}\ {}^1\Sigma^+\right)$ and excited $\left({}^1\Sigma^-,\ {}^1\Delta\right)$ states of HCP and HPC have been systematically investigated using *ab initio* molecular electronic structure theory. For the ground state, geometries of the two linear stationary points have been optimized and physical properties have been predicted utilizing restricted self-consistent field theory, coupled cluster theory with single and double excitations (CCSD), CCSD with perturbative triple corrections [CCSD(T)], and CCSD with partial iterative triple excitations (CCSDT-3 and CC3). Linear HPC, a stationary point of Hessian index 2, is predicted to lie 75.2 kcal mol^{-1} above the global minimum HCP. The dissociation energy D_0 $\left[HCP\left(\widetilde{X}\ {}^1\Sigma^+\right)\rightarrow H\left({}^2S\right)+CP\left(X\ {}^2\Sigma^+\right)\right]$ of HCP is predicted to be 119.0 kcal mol^{-1}, which is very close to the experimental lower limit of 119.1 kcal mol^{-1}. Eight singlet excited states were examined and their physical properties were determined employing three equation-of-motion coupled cluster methods (EOM-CCSD, EOM-CCSDT-3, and EOM-CC3). Four stationary points were located on the lowest-lying excited state potential energy surface, ${}^1\Sigma^-\rightarrow{}^1A''$, with excitation energies T_e of 101.4 kcal mol^{-1} $\left({}^1A''\ HCP\right)$, 104.6 kcal mol^{-1} $\left({}^1\Sigma^-\ HCP\right)$, 122.3 kcal mol^{-1} $\left({}^1A''\ HPC\right)$, and 171.6 kcal mol^{-1} $\left({}^1\Sigma^-\ HPC\right)$ at the cc-pVQZ EOM-CCSDT-3 level of theory. The physical properties of the ${}^1A''$ state with a predicted bond angle of 129.5° compare well with the experimentally reported first singlet state $\left(\widetilde{A}\ {}^1A''\ \right)$. The excitation energy predicted for this excitation is T_0=99.4 kcal mol^{-1} (34,800 cm^{-1}, 4.31 eV), in essentially perfect agreement with the experimental value of T_0=99.3 kcal mol^{-1} (34,746 cm^{-1}, 4.308 eV). For the second lowest-lying excited singlet surface, ${}^1\Delta\rightarrow{}^1A'$, four stationary points were found with T_e values of 111.2 kcal mol^{-1} $\left(2{}^1A'\ HCP\right)$, 112.4 kcal mol^{-1} $\left({}^1\Delta\ HPC\right)$, 125.6 kcal mol^{-1} $\left(2\ {}^1A'\ HCP\right)$, and 177.8 kcal mol^{-1} $\left({}^1\Delta\ HPC\right)$. The predicted CP bond length and frequencies of the $2\ {}^1A'$ state with a bond angle of 89.8° (1.707 Å, 666 and 979 cm^{-1}) compare reasonably well with those for the experimentally reported $\widetilde{C}\ {}^1A'$ state (1.69 Å, 615 and 969 cm^{-1}). However, the excitation

energy and bond angle do not agree well: theoretical values of 108.7 kcal mol^{-1} and 89.8° versus experimental values of 115.1 kcal mol^{-1} and 113°.

2.2 Introduction

The successful synthesis of phosphaethyne or methinophosphide (HCP) in 1961 by Gier was the first report of a molecule containing a multiple bond between phosphorus and carbon[1]. Gier observed bands in the infrared (IR) absorption spectrum that compared favorably to assumed C–H stretching frequencies and H–C–X bending frequencies. Failing to see any band in the region corresponding to a H–P bend, Gier concluded that the molecule was linear HCP and not HPC. In 1964, Tyler[2] reported the microwave spectrum of HCP and concurred with the conclusion of Gier[1]. The dipole moment (0.39 polarity $^{+}HCP^{-}$) and bond lengths (1.067 and 1.542 Å) of the ground state $\left(^1\Sigma^+\right)$ were determined by Tyler. HCP is of astrophysical interest owing to its presence in the interstellar medium and the atmosphere of Saturn[3-5].

The ultraviolet (UV) spectrum of HCP was first reported in an extensive spectroscopic study by Johns *et al.* in 1969[6]. They deduced ground state information using their own rovibronic analysis along with data from Tyler's earlier microwave study[2]. Fundamental vibrational frequencies for the symmetric and asymmetric stretching and the bending modes were reported as 3217 $cm^{-1}\left(\nu_1\right)$, 1278 $cm^{-1}\left(\nu_3\right)$, and 675 $cm^{-1}\left(\nu_2\right)$, respectively. Also, the CP bond length was reported as 1.542 Å, in agreement with that of Tyler. Seven excited electronic states were identified, including three singlet states of interest, with electronic excitation energies (T_0) of 34,750 cm^{-1} (99.3 kcal mol^{-1}) for $\widetilde{A}\ ^1A''$, 35,930 cm^{-1} (102.7 kcal mol^{-1}) for $\widetilde{B}\ ^1\Pi$, and 40,250 cm^{-1} (115.1 kcal mol^{-1}) for $\widetilde{C}\ ^1A'$, as well as four triplet states. For the $\widetilde{A}$ and $\widetilde{C}$ states, values of ν_2 were found to be 567 and 615 cm^{-1} and values of ν_3 to be 954 and 969 cm^{-1}, respectively.

The second singlet excited state $\left(\widetilde{B}\right)$, considered by Johns *et al.*[6] to be a $^1\Pi$ state, was reexamined in 1972 by Moehlmann *et al.*[7] in a study exploiting the Zeeman effect. The group found

that the Zeeman splitting for the $\widetilde{B}$ state increased as the rotational quantum number *J* increases. This sort of behavior is not expected of a $^1\Pi$ state, and Moehlmann *et al.* concluded that the excited state described as $\widetilde{B}$ was actually a $^3\Delta$ state. Later that year the same group, utilizing the Stark effect, determined the dipole moment of the first $^1A''$ state of HCP to be 0.44±0.06 D (polarity not determined). In 1973 Frost *et al.*[8] measured the photoelectron spectrum of HCP and determined the energy required to remove an electron from the HOMO (2π) to be 10.8 eV. In 1999 Ishikawa *et al.*[9] reported results of an IR-UV double resonance spectroscopy study on HCP. They established a C–H stretching frequency of 2930 cm^{-1} for the $\widetilde{A}\ ^1A''$ state.

A series of IR studies[10-13] were conducted that appear to give fundamental stretching vibrational frequencies to greater precision than those reported by Johns *et al.*[6] Kalasinsky and Pechsiri[14] recorded the Raman spectrum in 1985 and determined the fundamental vibrational frequencies, ν_1=3218 cm^{-1} and ν_3=1277 cm^{-1}. Mason and Lehman[15] in 1993 measured the laser-induced fluorescence spectrum of HCP and found a sharp decrease in intensity at 41,680 cm^{-1}. They assigned this decrease in intensity to the coupling of excited vibrational levels with the dissociative continuum of the ground state. From their data they placed a lower limit on the dissociation energy at 41,650 cm^{-1} (119.1 kcal mol^{-1}).

A number of studies have been conducted with the intention of determining accurate structural parameters for the ground state of HCP. Using results obtained for HCN as constraints, Strey and Mills[16] in 1973 used vibration-rotation constants determined by Johns *et al.*[6] to deduce an anharmonic force field for HCP. From this data they determined r_e(HC)=1.0692(8) Å and r_e(CP)=1.5398(2) Å. In 1996, Dréan *et al.*[17] remeasured the rotational spectrum, determining zero-point rotational constants and values for r_0(HC) =1.0652 Å and r_0(CP)=1.5442 Å. Dréan *et al.* used rotational constants to extrapolate to equilibrium rotational constants yielding r_e(HC)=1.0670 Å and r_e(CP)=1.5402 Å. Ishikawa *et al.*[18] performed an algebraic analysis of intensities from the emission

spectrum of HCP. From their study, Ishikawa *et al.* reported r_e(HC)=1.067 Å and r_e(CP) =1.642 Å and a bond angle of 122.1° for the first $\tilde{A}\ ^1A''$ excited state.

Numerous theoretical studies have also been reported regarding the ground state parameters of HCP[19-38]. There have been three configuration interaction (CI) studies of the excited states of HCP. First, in 1990, Karna *et al.*[39] studied a number of singlet, triplet, and quintet and linear and bent excited states using the multireference configuration interaction single and double excitation (MRCISD) method including energy extrapolation. The linear singlet states of interest to the present study, with T_e in eV, are $^1\Sigma^-$ (4.57) and $^1\Delta$ (4.95). In accord with other groups, Karna *et al.* did not find a $^1\Pi$ state where Johns *et al.*[6] had reported. The bent structures Karna *et al.* characterized include the $^1A''$ (4.42) and $^1A'$ (4.9) states with a H–C–P bond angle of 131° and 140°, respectively. In 1993 Sannigrahi and Grein[40] described results of multireference double excitation configuration interaction (MRD-CI) calculations on the three lowest $^1A'$ and $^1A''$ states at a fixed CH distance of 1.071 Å. The three lowest $^1A'$ states corresponded (approximate T_e values in eV and bond angles) to $^1\Sigma^+$ (0.0, 180.0°), $^1\Delta$ (4.60, 93°), and $^1\Sigma^+$ (6.25, 105.0°) and the three lowest $^1A''$ states to $^1\Sigma^-$ (4.45, 126.0°), $^1\Delta$ (5.00, 180.0°), and $^1\Delta$ (7.10, 116.0°). The third CI study was performed by Nanbu *et al.*[41] in 2000, utilizing DZP and aug-cc-pVDZ basis sets with MRCISD based on a complete active space self-consistent field (CASSCF) reference wave function. The latter group was the first to characterize excited states that more closely resemble HPC than HCP. They distinguished two $^1A''$ states arising from $^1\Sigma^-$ and $^1\Delta$, plus three $^1A'$ minima and one $^1A''$ minimum. The group found that even though the ground state does not exhibit any stable linear minima on the HPC side, both the $^1\Sigma^-$ and $^1\Delta$ states lead to bent minima resembling HPC.

One other theoretical study of interest concerning HCP singlet excited states was reported in 1993 with work by Goldstein *et al.*[42] Geometries were optimized with Møller-Plesset second-order perturbation theory (MP2) for the ground state while CASSCF was utilized to study the excited states. The study of Goldstein *et al.* reported that linear HCP and linear HPC are minima with a bent transition state occurring near θ(HPC)=136° with respect to the HPC angle. The only singlet state discussed in their

study was the aforementioned $^1A''$ state derived from linear $^1\Sigma^-$ at 4.80 eV (with their largest basis, TZV++, and CASSCF configuration space, ten electrons in ten molecular orbitals).

Early experimental studies do not mention the possibility that linear HPC exists[1,2,6,8,10-14]. A later study by Lehmann *et al.*[43] in 1985 found that a fit of vibrational levels of the ground state gives a description of the bending potential from 0° (linear HCP) to 100°. The fit gives no indication that a turnover will occur causing a minimum for HPC. There was much controversy by early theoretical investigations regarding the true nature of HPC. It was previously mentioned that Goldstein *et al.*[42] determined linear HPC to be a local minimum through the use of MP2 theory. The potential energy surface of the ground state was once again studied in 1993 by Ma *et al.*[44], who found MP2 and MP4 to give local minima while MP3 found a saddle point for the linear HPC conformation. Hong and Cave[45] in 1994 concluded that HPC has considerably more multireference character than HCP. The results of CASSCF and CCSD wave functions both reveal linear HPC to be a saddle point with the use of a small basis set (6–311G). The MRCI method was utilized by Beck *et al.*[46] to determine a potential energy surface for the ground state, leading to the conclusion that HPC is an energetic maximum with respect to bending. Much of what has been stated about the HPC→HCP isomerization has been reviewed in an important paper by Ishikawa *et al.*[47]

The goals of the present study are twofold. Potential energy surfaces of the ground and low-lying singlet excited states of HCP will be constructed as an aid to uncovering minima and saddle points. The ground state energies, geometries, dipole moments, and harmonic vibrational frequencies will be determined for both the linear HCP and HPC configurations in the ground state. These two conformations, from previous work, likely constitute the global minimum and a local maximum, respectively. Secondly, the low-lying singlet excited states of both linear and bent geometries will be explored using a variety of equation-of-motion (EOM) coupled cluster techniques. This will be conducted for states arising from both the HCP and HPC regions of the potential energy surface. The results will be compared to previous experimental and theoretical studies.

2.3 Electronic Structure Considerations

The electronic configurations of the linear $\widetilde{X}\ ^1\Sigma^+$ ground states of HCP and HPC are qualitatively described as

$$[core](5\sigma)^2(6\sigma)^2(7\sigma)^2(2\pi)^4 \quad \widetilde{X}\ ^1\Sigma^+ \tag{1}$$

where (core) denotes the carbon 1*s*-like molecular orbital and the phosphorus 1*s*-, 2*s*-, and 2*p*-like orbitals. Let π_x and π_y be π molecular orbitals (MOs) in real coordinates, denoting the π components in the *xz* plane and *yz* plane (the *z* axis is assigned to the molecular axis). Configuration 1 may be written in real orbital form

$$[core](5\sigma)^2(6\sigma)^2(7\sigma)^2(2\pi_x)^2(2\pi_y)^2 \quad \widetilde{X}\ ^1\Sigma^+ \tag{2}$$

The lowest-lying excited electronic states for HCP/HPC are obtained conceptually by exciting an electron from the bonding 2π [highest occupied molecular orbital (HOMO)] orbital to the antibonding 3π [lowest unoccupied molecular orbital (LUMO)] orbital. This gives rise to three excited singlet states of HCP and HPC for linear geometries,

$$[core](5\sigma)^2(6\sigma)^2(7\sigma)^2(2\pi)^3(3\pi)^1 \quad {}^1\Sigma^+, {}^1\Sigma^-, {}^1\Delta \tag{3}$$

The electronic configuration of the $^1\Delta$ state requires four Slater determinants in real MO notation. Assuming the molecule lies on the *z* axis, the two $^1\Delta$ components ($^1A_1$ and $^1A_2$ in C_{2v} subgroup, respectively) are

$$\begin{aligned}[core](5\sigma)^2(6\sigma)^2(7\sigma)^2\big[&(2\pi_x\alpha)(2\pi_y)^2(3\pi_x\beta)\\ &+(2\pi_x)^2(2\pi_y\beta)(3\pi_y\alpha)-(2\pi_x\beta)(2\pi_y)^2(3\pi_x\alpha)\\ &-(2\pi_x)^2(2\pi_y\alpha)(3\pi_y\beta)\big]\end{aligned} \tag{4}$$

and

$$\begin{aligned}[core](5\sigma)^2(6\sigma)^2(7\sigma)^2\big[&(2\pi_x\alpha)(2\pi_y)^2(3\pi_y\beta)\\ &+(2\pi_x)^2(2\pi_y\alpha)(3\pi_x\beta)-(2\pi_x\beta)(2\pi_y)^2(3\pi_y\alpha)\\ &-(2\pi_x)^2(2\pi_y\beta)(3\pi_x\alpha)\big]\end{aligned} \tag{5}$$

The open-shell part of the $^1\Sigma^-$ state also requires four Slater determinants in real MO notation,

$$\begin{aligned}&[core](5\sigma)^2(6\sigma)^2(7\sigma)^2\left[(2\pi_x\alpha)(2\pi_y)^2(3\pi_y\beta)\right.\\&+(2\pi_x)^2(2\pi_y\beta)(3\pi_x\alpha)-(2\pi_x\beta)(2\pi_y)^2(3\pi_y\alpha)\\&\left.-(2\pi_x)^2(2\pi_y\alpha)(3\pi_x\beta)\right]\end{aligned} \tag{6}$$

2.4 Theoretical Methods

Five correlation-consistent polarized-valence basis sets developed by Dunning and co-workers[48-50], cc-pVXZ (X =T,Q,5) and aug-cc-pVXZ (X=T,Q), were utilized in this study. The largest basis set, cc-pV5Z, consisted of 241 contracted Gaussian functions. Geometries were optimized with each basis set and level of theory. Harmonic vibrational frequencies were determined using analytic methods when available and otherwise through finite differences of analytic gradients or numerical differentiation of total energies.

The zeroth-order description of the ground state was obtained using restricted Hartree-Fock (RHF) self-consistent field theory (SCF). The effects of electron correlation were then included for the ground state molecules using coupled cluster (CC) theory with single and double excitations (CCSD)[51,52], the inclusion of perturbative triple excitations [CCSD(T) (Ref. 53, 54)], and with two methods for partial iterative triples [CCSDT-3 (Ref. 55) and CC3 (Ref.. 56)]. To investigate the excited electronic states, three equation-of-motion coupled cluster (EOM-CC) methods[57,58] were utilized (EOM-CCSD, EOM-CCSDT-3, and EOM-CC3). For these correlated methods, six core orbitals were frozen, namely, the 1*s*-like orbital of carbon and the 1*s*-, 2*s*-, and 2*p*-like orbitals of phosphorus. The *ab initio* quantum chemistry packages utilized in this study include ACESII[59] and MOLPRO[60].

2.5 Results

In Figure 2.1 the stationary points optimized are schematically depicted using excitation energies (T_e) determined with the cc-pVQZ basis set at the CCSDT-3 level of theory for the ground state and EOM-CCSDT-3 for the excited states. For the $\widetilde{X}\ ^1\Sigma^+$ states of HCP and HPC, the total energies, frequencies, and dipole moments can be found in Tables 2.1 and 2.2 and the bond lengths in Figures 2.2 and 2.3, respectively. Energy differences between the two ground state isomers and dissociation energies are

reported in Table 2.3. For the $^1\Sigma^-$ states, the total energies, bond lengths, and excitation energies are summarized in Tables 2.4 and 2.7. The total energy and harmonic vibrational frequencies of the HCP and HPC $^1A''$ states arising from $^1\Sigma^-$ are given in Tables 2.5 and 2.6, with optimized geometries and angles in Figures 2.4 and 2.5. For the $^1\Delta$ states, the energy, bond lengths, and excitation energies are summarized in Tables 2.8 and 2.11. The total energy and harmonic vibrational frequencies of the HCP and HPC $^1A'$ states arising from $^1\Delta$ are given in Tables 2.9 and 2.10 with optimized geometries in Figures 2.6 and 2.7.

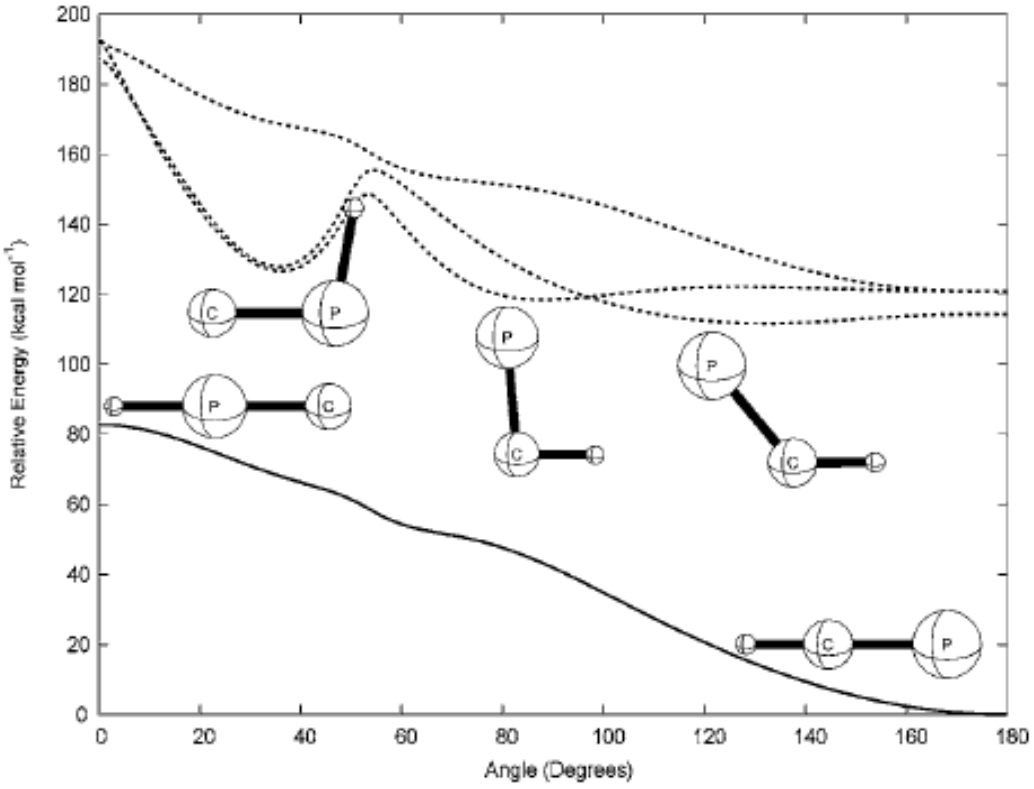

Figure 2.1: Ten stationary points determined in this study. Energies reported in diagram are with the cc-pVQZ basis set utilizing CCSD level of theory for the ground state and EOM-CCSD level of theory for the excited states. There is no attempt to depict barriers in this figure.

2.5.1 $\widetilde{X}\ ^1\Sigma^+$ ground states of HCP and HPC

HCP in Figure 2.2 and HPC in Figure 2.3 exhibit elongation of the two bonds upon augmentation of the basis set and a decrease in bond length with increases in the size of the basis set. More advanced treatments of correlation effects induce a lengthening of both bond distances for each ground state isomer. Overall, smaller changes are found for the CH and PH bonds than the CP bond upon increasing the size of the basis. As bond lengths decrease, the vibrational frequency will tend to increase, which is consistent with Badger's rule[61,62] that the larger force constant (higher vibrational frequency) may be associated with the shorter bond length. The vibrational frequencies generally decrease with the inclusion of diffuse functions, increase when changing the basis from triple to quadruple zeta, and decrease with increasing sophistication in the treatment of electron correlation. The magnitude of the dipole moment (direction $^+$HCP$^-$) tends to decrease with the basis set size and increase with electron correlation with the opposite effect occurring for the IR intensities.

The present theoretical predictions provide excellent agreement with the equilibrium values of the bond lengths reported in previous experimental studies[16-18]. The CCSD(T) CH bond length differs by 0.003 Å from the equilibrium bond lengths determined from the experimental anharmonic force field of Strey and Mills[16]. There is a larger distinction for the CP bond lengths; for example, SCF with the cc-pV5Z basis still differs by roughly 0.04 Å but only by 0.004 Å from experiment with cc-pV5Z CCSD(T). Excellent agreement was also obtained for the cc-pV5Z values of ω_2 and ω_3 for HCP, which agree with the experimental fundamentals to within 20 cm^{-1}. The calculated value of ω_1 agrees with experiment to within 130 cm^{-1} at the highest level of theory, but this sort of discrepancy is expected as we are comparing harmonic to fundamental vibrational frequencies.

As mentioned previously, HPC has never been realized experimentally. This is nicely explained by the rearrangement of HCP to HPC being a monotonically uphill process with HPC serving as a stationary point of Hessian index 2. Table 2.2 summarizes the theoretical results for HPC. The second-order saddle point can be seen from the degenerate imaginary frequencies for the bending mode, denoted

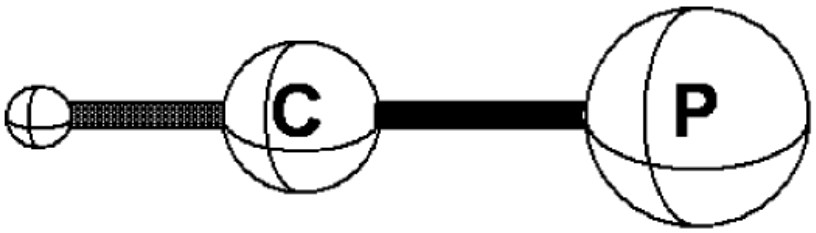

cc-pVTZ SCF	1.0615	1.5131	
aug-cc-pVTZ SCF	1.0615	1.5134	
cc-pVQZ SCF	1.0611	1.5096	
aug-cc-pVQZ SCF	1.0611	1.5097	
cc-pV5Z SCF	1.0610	1.5079	
cc-pVTZ CCSD	1.0705	1.5433	
aug-cc-pVTZ CCSD	1.0710	1.5438	
cc-pVQZ CCSD	1.0698	1.5367	
aug-cc-pVQZ CCSD	1.0699	1.5370	
cc-pV5Z CCSD	1.0696	1.5339	
cc-pVTZ CCSD(T)	1.0728	1.5540	
aug-cc-pVTZ CCSD(T)	1.0734	1.5547	
cc-pVQZ CCSD(T)	1.0722	1.5473	
aug-cc-pVQZ CCSD(T)	1.0723	1.5477	
cc-pV5Z CCSD(T)	1.0720	1.5445	
cc-pVTZ CCSDT-3	1.0727	1.5533	
aug-cc-pVTZ CCSDT-3	1.0732	1.5540	
cc-pVQZ CCSDT-3	1.0720	1.5467	
aug-cc-pVQZ CCSDT-3	1.0721	1.5471	
cc-pVTZ CC3	1.0732	1.5552	
aug-cc-pVTZ CC3	1.0737	1.5559	
cc-pVQZ CC3	1.0725	1.5486	
aug-cc-pVQZ CC3	1.0726	1.5490	
Experiment Ref. (5)	1.0667	1.5421	(r_0)
Experiment Ref. (16)	1.0692	1.5398	(r_e)
Experiment Ref. (17)	1.0670	1.5402	(r_e)
Experiment Ref. (18)	1.067	1.542	(r_e)

Figure 2.2: Predicted geometries of the global minimum HCP $\left({}^1\Sigma^+\right)$. Bond lengths are in Å.

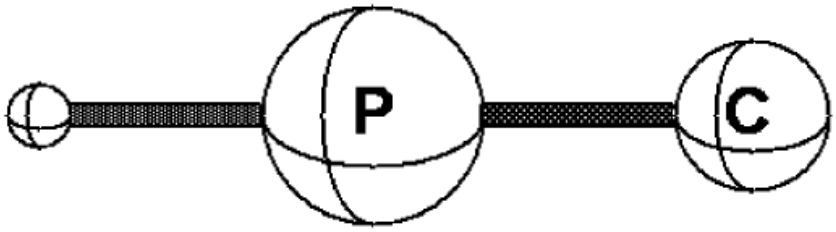

cc-pVTZ SCF	1.3879	1.5738
aug-cc-pVTZ SCF	1.3880	1.5739
cc-pVQZ SCF	1.3868	1.5708
aug-cc-pVQZ SCF	1.3868	1.5709
cc-pV5Z SCF	1.3864	1.5695
cc-pVTZ CCSD	1.4145	1.6076
aug-cc-pVTZ CCSD	1.4147	1.6081
cc-pVQZ CCSD	1.4124	1.6014
aug-cc-pVQZ CCSD	1.4128	1.6017
cc-pV5Z CCSD	1.4116	1.5989
cc-pVTZ CCSD(T)	1.4243	1.6255
aug-cc-pVTZ CCSD(T)	1.4247	1.6262
cc-pVQZ CCSD(T)	1.4224	1.6189
aug-cc-pVQZ CCSD(T)	1.4229	1.6194
cc-pV5Z CCSD(T)	1.4216	1.6163
cc-pVTZ CCSDT-3	1.4225	1.6260
aug-cc-pVTZ CCSDT-3	1.4229	1.6266
cc-pVQZ CCSDT-3	1.4207	1.6195
aug-cc-pVQZ CCSDT-3	1.4211	1.6199
cc-pVTZ CC3	1.4247	1.6314
aug-cc-pVTZ CC3	1.4252	1.6320
cc-pVQZ CC3	1.4229	1.6247
aug-cc-pVQZ CC3	1.4235	1.6251

Figure 2.2: Predicted geometries of the linear stationary point HPC $\left(^1\Sigma^+\right)$. Bond lengths are in Å.

Table 2.1: HCP total energies (in Hartree), dipole moments (in Debye), harmonic vibrational frequencies (in cm^{-1}), IR intensities (in km mol^{-1}), and zero-point vibrational energies (ZPVE in kcal mol^{-1}) for the ground state $\left(\widetilde{X}\ ^1\Sigma^+\right)$. IR intensities of the ω_2 mode were doubled.

Level of Theory	Total Energy	μ_e	$\omega_1(\sigma^+)$	$\omega_2(\pi)$	$\omega_3(\sigma^+)$	ZPVE
cc-pVTZ SCF	-379.151513	0.397	3514(20)	825(178)	1464(2)	9.48
aug-cc-pVTZ SCF	-379.152314	0.369	3514(21)	821(183)	1461(1)	9.46
cc-pVQZ SCF	-379.158888	0.359	3514(19)	827(183)	1466(2)	9.48
aug-cc-pVQZ SCF	-379.159062	0.346	3513(20)	827(182)	1465(1)	9.48
cc-pV5Z SCF	-379.161261	0.331	3515(19)	829(185)	1467(1)	9.49
cc-pVTZ CCSD	-379.463704	0.424	3374(15)	709(144)	1331(0.3)	8.75
aug-cc-pVTZ CCSD	-379.468093	0.397	3366(15)	699(144)	1328(0.07)	8.71
cc-pVQZ CCSD	-379.485516	0.396	3376(15)	714(146)	1341(0.3)	8.78
aug-cc-pVQZ CCSD	-379.487227	0.382	3374(15)	713(144)	1340(0.2)	8.78
cc-pV5Z CCSD	-379.492936	0.373	3376(15)	716(146)	1345(0.3)	8.80
cc-pVTZ CCSD(T)	-379.483951	0.481	3345(13)	682(138)	1285(0.3)	8.57
aug-cc-pVTZ CCSD(T)	-379.488961	0.451	3336(13)	672(138)	1281(0.08)	8.52
cc-pVQZ CCSD(T)	-379.507249	0.454	3345(13)	687(140)	1295(0.3)	8.60
aug-cc-pVQZ CCSD(T)	-379.509192	0.439	3343(13)	685(138)	1293(0.2)	8.59
cc-pV5Z CCSD(T)	-379.515185	···	3344	689	1298	8.61
cc-pVTZ CCSDT-3	-379.482848		3347	686	1287	8.59
aug-cc-pVTZ CCSDT-3	-379.487831		3338	675	1284	8.54
cc-pVQZ CCSDT-3	-379.506256		3347	690	1297	8.61
aug-cc-pVQZ CCSDT-3	-379.508204		3345	689	1296	8.60
cc-pVTZ CC3	-379.485136		3341	682	1278	8.55
aug-cc-pVTZ CC3	-379.490172		3332	671	1275	8.50
cc-pVQZ CC3	-379.508588		3341	686	1288	8.58
aug-cc-pVQZ CC3	-379.510549		3339	685	1286	8.57

	μ_0	ν_1	ν_2	ν_3
Experiment Ref. 2	0.390			
Experiment Ref. 6		3216.9	674.7	1278.4
Experiment Ref. 14		3218		1277

Table 2.2: HPC total energies (in Hartree), dipole moments (in Debye), harmonic vibrational frequencies (in cm^{-1}), IR intensities (in km mol^{-1}), and zero-point vibrational energies (ZPVE in kcal mol^{-1}) for the ground state $\left(\widetilde{X}\ ^1\Sigma^+\right)$.

Level of Theory	Total Energy	μ_e	$\omega_1(\sigma^+)$	$\omega_2(\pi)$	$\omega_3(\sigma^+)$	ZPVE
cc-pVTZ SCF	-379.003969	4.111	2641(35)	658i	1306(130)	5.64
aug-cc-pVTZ SCF	-379.004700	4.131	2638(37)	662i	1302(133)	5.63
cc-pVQZ SCF	-379.010142	4.153	2639(36)	669i	1306(135)	5.64
aug-cc-pVQZ SCF	-379.010295	4.158	2638(36)	671i	1305(135)	5.64
cc-pV5Z SCF	-379.011883	4.172	2638(35)	673i	1306(136)	5.64
cc-pVTZ CCSD	-379.332917	3.462	2395(5)	424i	1185(64)	5.12
aug-cc-pVTZ CCSD	-379.337446	3.506	2392(4)	430i	1180(68)	5.11
cc-pVQZ CCSD	-379.353468	3.531	2401(3)	438i	1193(69)	5.14
aug-cc-pVQZ CCSD	-379.355257	3.543	2399(3)	439i	1191(70)	5.13
cc-pV5Z CCSD	-379.360300	···	2402	441i	1196	5.14
cc-pVTZ CCSD(T)	-379.359868	3.202	2308(23)	337i	1112(60)	4.89
aug-cc-pVTZ CCSD(T)	-379.365108	3.239	2303(4)	344i	1109(63)	4.88
cc-pVQZ CCSD(T)	-379.382057	3.263	2313(19)	351i	1123(64)	4.91
aug-cc-pVQZ CCSD(T)	-379.384119	3.272	2310(19)	352i	1121(64)	4.90
cc-pV5Z CCSD(T)	-379.389496	···	2313	353i	1126	4.92
cc-pVTZ CCSDT-3	-379.358591		2324	356i	1103	4.90
aug-cc-pVTZ CCSDT-3	-379.363788		2319	363i	1100	4.89
cc-pVQZ CCSDT-3	-379.380930		2328	369i	1113	4.92
aug-cc-pVQZ CCSDT-3	-379.382995		2325	370i	1112	4.91
cc-pVTZ CC3	-379.362618		2304	338i	1077	4.83
aug-cc-pVTZ CC3	-379.367898		2304	338i	1077	4.83
cc-pVQZ CC3	-379.385022		2308	351i	1088	4.85
aug-cc-pVQZ CC3	-379.387108		2305	352i	1086	4.85

$\omega_2(\pi)$. The CP bond lengthens by nearly a tenth of an angstrom in going from HCP to HPC. The two stretching frequencies, ω_1 and ω_3, are lower for HPC than for HCP due to the weakening and subsequent lengthening of the two bonds. HPC has an imaginary bending frequency roughly half the magnitude of the real bending frequency for HCP. There is a considerable increase in the dipole moment (direction $^{+}$HCP^{-}) for HPC owing mainly to the greater electronegativity of the carbon atom now situated at the end of the molecule.

The relative energy differences between HCP and HPC and the dissociation energies defined by $HCP\left(\widetilde{X}\ ^1\Sigma^+\right) \rightarrow H\left(^2S\right) + CP\left(X\ ^2\Sigma^+\right)$ are found in Table 2.3. At the highest level of theory, the energy differences between HCP and HPC with and without zero-point vibrational energy (ZPVE) corrections are 78.9 and 75.2 kcal mol^{-1}, respectively. The best previous theoretical energy separation is 79.1 kcal mol^{-1}, in good agreement with our value. The previous MP*n* calculations, with small basis sets, do a mediocre job of describing this energy difference.

The experimental dissociation energy of 119.1 kcal mol^{-1} by Mason and Lehmann was candidly reported as uncertain. Our ZPVE corrected value of 119.0 kcal mol^{-1} at the cc-pV5Z CCSD(T) level of theory provides strong support for their result. The SCF method underestimates the experimental value by 18 kcal mol^{-1}, but the inclusion of electron correlation with the CC methods apparently provides a very good estimation of the experimental value.

2.5.2 Excited States

2.5.2.1 Lowest $^1\Sigma^-$ state of HCP

Three low-lying excited singlet states arise from the excitation of an electron from the 2π to 3π orbital [Eq. 3, above]. The lowest energy state arising from this promotion is a $^1\Sigma^-$ electronic state. The linear HCP conformation of this excitation is found to be a stationary point of Hessian index 2. The CH bond length in Table 2.4 changes by no more than 0.001 Å for this electronic state, while the CP bond length increases by more than 0.1 Å relative to the ground state of HCP at each level of theory. This trend can

Table 2.3: Relative energies (in kcal mol^{-1}) of the ground states of HCP and HPC (ΔE of linear HCP and linear HPC). Dissociation energies (in kcal mol^{-1}) of linear HCP $\left(\tilde{X}\ ^1\Sigma^+\right)$ into atomic H (^{2}S) and CP $\left(^2\Sigma^+\right)$. Zero-point vibrational energy corrected values in parentheses.

Level of Theory	E(HPC) - E(HCP)	Dissociation Energy
cc-pVTZ SCF	92.6(88.8)	109.0(101.6)
aug-cc-pVTZ SCF	92.6(88.8)	109.1(101.6)
cc-pVQZ SCF	93.3(89.5)	109.1(101.7)
aug-cc-pVQZ SCF	93.4(89.5)	109.1(101.7)
cc-pV5Z SCF	93.7(89.9)	109.3(101.9)
cc-pVTZ CCSD	82.1(78.4)	124.8(117.8)
aug-cc-pVTZ CCSD	82.0(78.4)	125.1(118.3)
cc-pVQZ CCSD	82.9(79.2)	126.0(119.1)
aug-cc-pVQZ CCSD	82.8(79.2)	126.1(119.2)
cc-pV5Z CCSD	83.2(79.6)	126.4(119.4)
cc-pVTZ CCSD(T)	77.9(74.2)	124.1(117.3)
aug-cc-pVTZ CCSD(T)	77.7(74.1)	125.5(118.6)
cc-pVQZ CCSD(T)	78.6(74.9)	125.5(118.6)
aug-cc-pVQZ CCSD(T)	78.5(74.8)	125.5(118.7)
cc-pV5Z CCSD(T)	78.9(75.2)	125.9(119.0)
cc-pVTZ CCSDT-3	78.0(74.3)	124.0(117.2)
aug-cc-pVTZ CCSDT-3	77.8(74.2)	124.4(117.7)
cc-pVQZ CCSDT-3	78.6(75.0)	125.3(118.5)
aug-cc-pVQZ CCSDT-3	78.6(74.9)	125.4(118.6)
cc-pVTZ CC3	76.9(73.2)	
aug-cc-pVTZ CC3	76.7(73.0)	
cc-pVQZ CC3	77.5(73.8)	
aug-cc-pVQZ CC3	77.5(73.7)	
MP4/6-31G**//HF/6-31G* Ref. 4	84.1	
MP2/6-311G**//MP4/6-311G** Ref. 5	93.6	
QCISCD(T)/6-31G(d,p) Ref. 6	79.6	
Experiment Ref. 7		119.1

be explained by the fact that the 2π orbital is composed of π-bonding and the 3π orbital of π-antibonding character between the carbon and phosphorus atoms, leading to little change in the CH bond distance but a considerable lengthening of the CP bond. The $^1\Sigma^-$ state is predicted to lie 104.6 kcal mol^{-1} above $\widetilde{X}\ ^1\Sigma^+$ HCP at the cc-pVQZ EOM-CCSDT-3 level of theory. A previous theoretical study by Karna *et al.*[39] gave excitation energies similar to our values. Their CP bond length is longer (0.005 Å) than our value, while the values of the CH bond length are very close.

Table 2.4: Total energies (in hartree), bond lengths (in Å), and electronic excitation energies T_e (in kcal mol^{-1}) for the linear $1\ ^1\Sigma^-$ state of HCP.

Level of theory	Total energy	r_e (HC)	r_e (CP)	T_e
cc-pVTZ EOM-CCSD	−379.292778	1.6593	1.0702	107.3
aug-cc-pVTZ EOM-CCSD	−379.299339	1.6597	1.0711	105.9
cc-pVQZ EOM-CCSD	−379.315206	1.6522	1.0694	106.9
cc-pVTZ EOM-CCSDT-3	−379.315449	1.6771	1.0726	105.0
aug-cc-pVTZ EOM-CCSDT-3	−379.322783	1.6776	1.0737	103.6
cc-pVQZ EOM-CCSDT-3	−379.339608	1.6695	1.0720	104.6
cc-pVTZ EOM-CC3	−379.317836	1.6809	1.0733	105.0
aug-cc-pVTZ EOM-CC3	−379.325255	1.6814	1.0745	103.5
cc-pVQZ EOM-CC3	−379.342023	1.6731	1.0727	104.5
MRD-CI (Ref.. 39)		1.677	1.079	105

2.5.2.2 Lowest $^1A''$ state of HCP

With only planar (C_s) symmetry, the $^1\Sigma^-$ state becomes $^1A''$ upon bending. The excitation corresponding to this $^1A''$ state is $2a'' \rightarrow 10a'$. According to Walsh's diagram for HAB molecules[63], an electron added to the $10a'$ orbital of HCP will cause a decrease in energy upon bending. The behavior reported in this study is consistent with Walsh's rules. The $^1A''$ state total energies and vibrational frequencies are summarized in Table 2.5, with geometrical parameters given in Fig. 2.3. Upon bending $\left(^1\Sigma^- \rightarrow {}^1A''\right)$, the

two bond lengths increase by 0.020 Å (CH) and 0.026 Å (CP) relative to the linear $\left(^1\Sigma^-\right)$ stationary point. At the best level of theory, T_e=101.4 kcal mol^{-1} and T_0=99.4 kcal mol^{-1} are predicted, in excellent agreement with an experimental observation of T_0=99.3 kcal mol^{-1} (34,746 cm^{-1}) by Johns *et al.*[6] for the $\widetilde{A}\ ^1A''$ state. Excellent agreement occurs between the theoretical ω_3 and the experimentally reported ν_3 vibrational modes, while the value of ω_1 is lower by roughly 130 cm^{-1} due to anharmonic effects. With the exception of ω_1, our theoretical frequencies are in better agreement with experimental values than those reported in previous theoretical studies[39,42].

Table 2.5: HCP total energies (in hartree), harmonic vibrational frequencies (in cm^{-1}), zero-point vibrational energies (ZPVE, in kcal mol^{-1}), and electronic excitation energies T_e and T_0 (in kcal mol^{-1}) for the $^1A''\left(^1\Sigma^-\right)$ state of HCP relative to $\widetilde{X}\ ^1\Sigma^+$ HCP.

Level of theory	Total energy	$\omega_1(a')$	$\omega_2(a')$	$\omega_3(a')$	ZPVE	T_e	T_0
cc-pVTZ EOM-CCSD	−379.297481	3102	569	989	6.66	104.3	102.2
aug-cc-pVTZ EOM-CCSD	−379.303644	3103	557	84	6.64	103.2	101.1
cc-pVQZ EOM-CCSD	−379.319188	3120	564	1002	6.70	104.4	102.3
cc-pVTZ EOM-CCSDT-3	−379.321328	3063	636	968	6.67	101.4	99.5
aug-cc-pVTZ EOM-CCSDT-3	−379.328149	3062	624	963	6.65	100.2	98.3
cc-pVQZ EOM-CCSDT-3	−379.344735	3076	628	977	6.69	101.4	99.4
cc-pVTZ EOM-CC3	−379.323862	3051	645	957	6.65	101.2	99.3
aug-cc-pVTZ EOM-CC3	−379.330838	3050	633	952	6.63	100.0	98.1
cc-pVQZ EOM-CC3	−379.347380	3064	636	966	6.67	101.2	99.3
MRD-CI (Ref.. 39)			669			101	
CASSCF/TZV++ (Ref.. 42)		2885	688	894		110	
MRD-CI (Ref.. 40)						99	
MRCI/aug-cc-pVDZ (Ref.. 41)						102	
	Total energy	ν_1	ν_2	ν_3	ZPVE	T_e	T_0
Experiment (Ref. 9)		2930					
Experiment (Ref. 6)		566.6		953.9			99.3

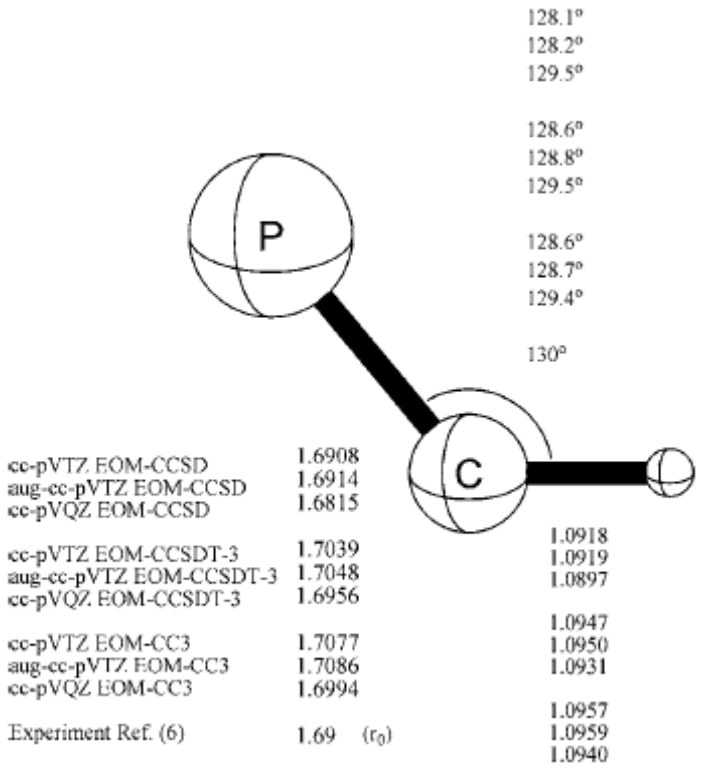

Figure 2.3: Predicted geometries of the $^1A''\left(^1\Sigma^-\right)$ state of HCP. Bond lengths are in Å. The experimental structure was deduced assuming r(C–H)=1.0667 Å.

2.5.2.3 Lowest $^1A''$ state of HPC

Further bending of the $^1A''$ state leads to another stable minimum at a HPC bond angle of approximately 98°. The barrier between this and the lowest $^1A''$ state of HCP lies 40.8 kcal mol^{-1} above the HCP minimum and 22.4 kcal mol^{-1} above the HPC minimum at the cc-pVQZ EOM-CCSD level of theory. Inspection of Figure 2.4 shows CP bond lengthening of nearly 0.1 Å with respect to the HCP minimum on this $^1A''$ surface. The $^1A''$ state of HPC is located at T_e=120.9 and T_0=117.5 kcal mol^{-1} relative to the ground state HCP. Thus we see that this $^1A''$ HPC structure lies approximately 20 kcal mol^{-1} above the analogous HCP structure. This state has been characterized by the previous theoretical study by Nanbu *et al.*[41] whose excitation energy is 3–5 kcal mol^{-1} higher than reported in this study, as seen in Table 2.6.

Spectroscopic observation of this state may prove challenging since the only stable minimum on the ground state surface is linear HCP, leading to an excitation that would lead the molecule first to the aforementioned bent $^1A''$ HCP minimum.

Table 2.6: HPC total energies (in hartree), harmonic vibrational frequencies (in cm^{-1}), zero-point vibrational energies (ZPVE, in kcal mol^{-1}), and electronic excitation energies T_e and T_0 (in kcal mol^{-1}) for the $^1A''\left(^1\Sigma^-\right)$ state of HPC relative to $\widetilde{X}\ ^1\Sigma^+$ HCP.

Level of theory	Total energy	$\omega_1(a')$	$\omega_2(a')$	$\omega_3(a')$	ZPVE	T_e	T_0
cc-pVTZ EOM-CCSD	−379.268779	2252	809	741	5.44	122.3	119.0
aug-cc-pVTZ EOM-CCSD	−379.274496	2251	809	743	5.44	121.5	118.2
cc-pVQZ EOM-CCSD	−379.289791	2259	819	751	5.48	122.8	119.5
cc-pVTZ EOM-CCSDT-3	−379.288885	2227	770	690	5.27	121.7	118.4
aug-cc-pVTZ EOM-CCSDT-3	−379.295187	2224	770	692	5.27	120.9	117.6
cc-pVQZ EOM-CCSDT-3	−379.311340	2216	762	683	5.23	122.3	117.5
cc-pVTZ EOM-CC3	−379.291088	2220	763	680	5.24	121.8	118.5
aug-cc-pVTZ EOM-CC3	−379.297458	2216	762	683	5.23	120.9	117.6
cc-pVQZ EOM-CC3	−379.313586	2225	770	690	5.27	122.4	119.1
MRCI/aug-cc-pVDZ (Ref.. 41)						125	

2.5.2.4 Lowest $^1\Sigma^-$ state of HPC

When the hydrogen atom is attached to the phosphorus atom and the molecule is linear, the $^1\Sigma^-$ state on the HPC side of the surface should be considered. This state is much higher in energy than any of the states discussed thus far. In fact, it has a T_e value of 172 kcal mol^{-1} relative to the HCP $\widetilde{X}\ ^1\Sigma^+$ minimum. This excitation energy places it nearly 70 kcal mol^{-1} higher in energy than its $^1\Sigma^-$ HCP counterpart. The excitation energy of this state when compared to the $^1\Sigma^+$ stationary point of HPC is 93 kcal mol^{-1} similar to the T_e value of $^1\Sigma^-$ HCP when compared to $\widetilde{X}\ ^1\Sigma^+$ HCP (104.6 kcal mol^{-1}). The HPC bond lengths for the $^1\Sigma^-$ state are similar for the PH separation, but the CP bond length increases by 0.184 Å in relation to $^1\Sigma^+$ HPC.

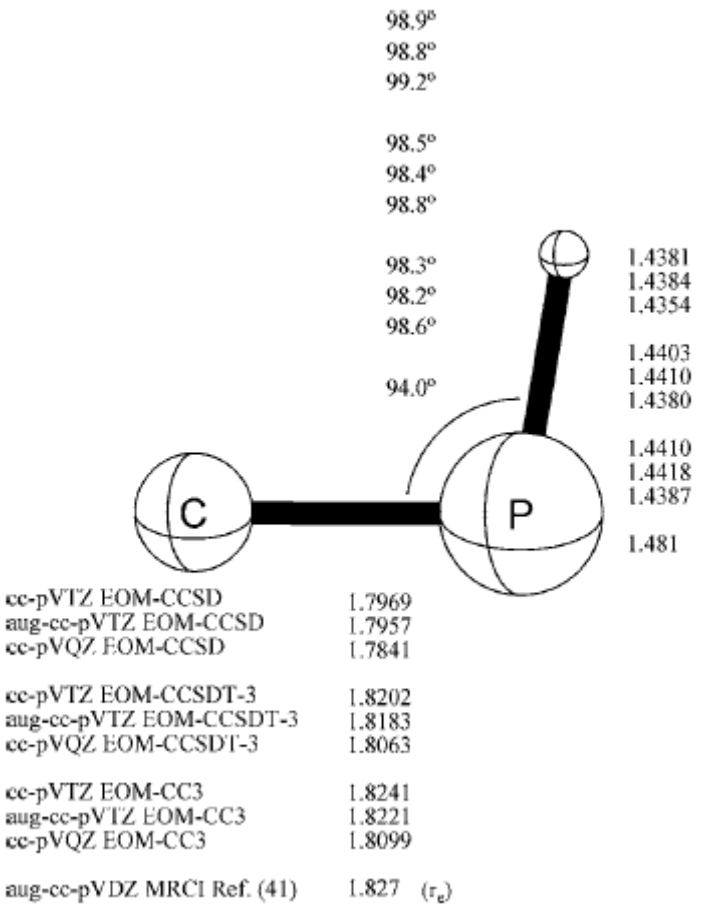

Figure 2.4: Predicted geometries of the $^1A''\left(^1\Sigma^-\right)$ state of HPC. Bond lengths are in Å.

Table 2.7: Total energies (in hartree), bond lengths (in Å), and electronic excitation energy T_e (in kcal mol^{-1}) for the linear $1\ ^1\Sigma^-$ state of HPC.

Level of theory	Total energy	r_e (HP)	r_e (CP)	T_e
cc-pVTZ EOM-CCSD	−379.180 927	1.4051	1.7781	177.5
aug-cc-pVTZ EOM-CCSD	−379.187 769	1.4067	1.7744	175.9
cc-pVQZ EOM-CCSD	−379.202 072	1.4039	1.7669	177.9
cc-pVTZ EOM-CCSDT-3	−379.209 798	1.4140	1.8133	171.3
aug-cc-pVTZ EOM-CCSDT-3	−379.217 489	1.4158	1.8101	169.6
cc-pVQZ EOM-CCSDT-3	−379.232 781	1.4130	1.8014	171.6
cc-pVTZ EOM-CC3	−379.214 370	1.4168	1.8270	169.9
aug-cc-pVTZ EOM-CC3	−379.222 192	1.4188	1.8237	168.2
cc-pVQZ EOM-CC3	−379.237 398	1.4158	1.8142	170.2

2.5.2.5 Lowest $^1\Delta$ state of HCP

For linear structures this electronic state has two degenerate components in C_s symmetry a $^1A'(9a' \rightarrow 10a')$ component and a $^1A''(9a' \rightarrow 3a'')$ component. Upon bending the two states are no longer degenerate, with the $^1A'$ component leading to an energetic minimum and the $^1A''$ component increasing in energy. This behavior is consistent with the Walsh diagram[63], where an excitation into the $9a'$ orbital lends itself to a bent configuration while an excitation into the $3a''$ orbital lends itself to a linear configuration. As seen in Table 2.8, the CH and CP bond lengths differ by less than 0.01 Å from previous work. The energy relative to the $\widetilde{X}\ ^1\Sigma^+$ state is T_e=112.4 kcal mol^{-1} at the cc-pVQZ EOM-CCSDT-3 level of theory. The excitation energies reported at the partial triples levels are as much as 2 kcal mol^{-1} lower in energy than those reported previously by MRD-CI.

Table 2.8: Total energies (in hartree), bond lengths (in Å), and *Te* (in kcal mol^{-1}) for the linear 1 $^1\Delta$ state of HCP.

Level of theory	Total energy	*Re* (CP)	r_e (HC)	T_e
cc-pVTZ EOM-CCSD	−379.280183	1.6502	1.0705	115.2
aug-cc-pVTZ EOM-CCSD	−379.287009	1.6597	1.0711	113.6
cc-pVQZ EOM-CCSD	−379.303092	1.6428	1.0697	114.5
cc-pVTZ EOM-CCSDT-3	−379.302519	1.6678	1.0730	113.2
aug-cc-pVTZ EOM-CCSDT-3	−379.310119	1.6776	1.0737	111.5
cc-pVQZ EOM-CCSDT-3	−379.327105	1.6598	1.0725	112.4
cc-pVTZ EOM-CC3	−379.305009	1.6718	1.0737	113.0
aug-cc-pVTZ EOM-CC3	−379.312671	1.6814	1.0745	111.4
cc-pVQZ EOM-CC3	−379.329596	1.6636	1.0732	112.3
MRD-CI (Ref.. 39)		1.672	1.079	114
MRD-CI (Ref.. 40)		1.675		115
MRCI/aug-cc-pVDZ (Ref.. 41)		1.662	1.080	123

Table 2.9: Total energies (in hartree), harmonic vibrational frequencies (in cm^{-1}), ZPVE (in kcal mol^{-1}), and electronic excitation energies T_e and T_0 (in kcal mol^{-1}) for the bent $^1A'(^1\Delta)$ state of HCP relative to $\widetilde{X}\ ^1\Sigma^+$ HCP.

Level of theory	Total energy	$\omega_1(a')$	$\omega_2(a')$	$\omega_3(a')$	ZPVE	T_e	T_0
cc-pVTZ EOM-CCSD	−379.281938	2757	555	970	6.12	114.1	111.4
aug-cc-pVTZ EOM-CCSD	−379.287825	2777	512	950	6.06	113.1	110.5
cc-pVQZ EOM-CCSD	−379.302800	2779	517	967	6.09	114.7	112.0
cc-pVTZ EOM-CCSDT-3	−379.306370	2647	683	977	6.16	110.7	108.3
aug-cc-pVTZ EOM-CCSDT-3	−379.312801	2661	643	957	6.09	109.8	107.4
cc-pVQZ EOM-CCSDT-3	−379.329048	2662	666	979	6.16	111.2	108.7
cc-pVTZ EOM-CC3	−379.309787	2612	723	998	6.19	110.0	107.7
aug-cc-pVTZ EOM-CC3	−379.316288	2624	693	976	6.14	109.1	106.8
cc-pVQZ EOM-CC3	−379.332549	2626	716	998	6.20	110.5	108.1
MRD-CI (Ref.. 39)						113	
MRD-CI (Ref.. 40)						106	
MRCI/aug-cc-pVDZ (Ref.. 41)						116	
Total energy		ν_1	ν_2	ν_3	ZPVE	T_e	T_0
Experiment (Ref. 6)			615.4	969.4			115.1

2.5.2.6 $2\ ^1A'$ state of HCP

As stated previously, the $^1A'$ component of the $^1\Delta$ state leads to a minimum (upon bending), occurring near a bond angle of 88°, as described by Fig. 2.5. The possibility exists that this is the state reported by Johns *et al.*[6] as $\widetilde{C}\ ^1A'$. Inspection of Table 2.9 shows that the agreement between theory and experiment for this state is not as good as for the $\widetilde{A}$ state, especially for the excitation energy. The $2\ ^1A'$ HCP excitation energy is T_e=111.2 and T_0=108.8 kcal mol^{-1} at the cc-pVQZ EOM-CCSDT-3 level of theory. The predicted T_0 value is about 6 kcal mol^{-1} below the experimental value[6]; however, there is reasonable agreement in the vibrational frequencies. The angles differ greatly but the CP bond length exhibits excellent agreement with the experimental values. The disagreement also involves the fact that we characterize the $2\ ^1A'$ state as arising from the $^1\Delta$ state, whereas experiment concludes that it comes

from a $^1\Sigma^+$ state. Other theoretical studies agree that this state arises from a $^1\Delta$ rather than a $^1\Sigma^+$ state[39-42].

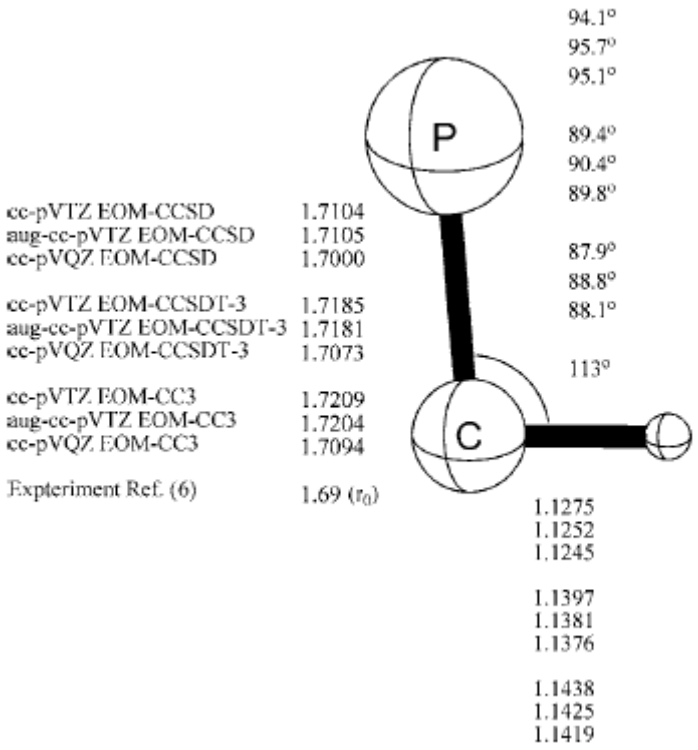

Figure 2.5: Predicted geometries of the $2\ ^1A'\left(^1\Delta\right)$ state of HCP. Bond lengths are in Å. The experimental structure was deduced assuming r(C–H)=1.0667 Å.

2.5.2.7 $2\ ^1A'$ state of HPC

The next state characterized in this study is seen as the hydrogen atom migrates along this same excited surface to a bent minimum more like HPC. The excitation energy compared to our global minimum is T_e=125.6 and T_0=122.2 kcal mol^{-1} at the cc-pVQZ EOM-CCSDT-3 level of theory. Our excitation energy for this state, similar to that for the $^1A''$ HPC state, is several kcal mol^{-1} below the theoretical value reported by Nanbu *et al.*[41] As was the case for the ground state isomers, the $2\ ^1A'$ state exhibits

a lengthening of the bonds as the hydrogen migrates from the carbon atom to the phosphorus atom. This leads to considerable decreases in the theoretical vibrational frequencies. This state should also be challenging to detect experimentally, with the well characterized linear HCP being the only minimum on the ground state potential energy surface.

Table 2.10: Total energies (in hartree), harmonic vibrational frequencies (in cm^{-1}), ZPVE (in kcal mol^{-1}), and T_e and T_0 values (in kcal mol^{-1}) for the $2\ ^1A'(^1\Delta)$ state of HPC relative to $\widetilde{X}\ ^1\Sigma^+$ HCP.

Level of theory	Total energy	$\omega_1(a')$	$\omega_2(a')$	$\omega_3(a')$	ZPVE	T_e	T_0
cc-pVTZ EOM-CCSD	−379.262558	2102	896	788	5.41	126.2	122.9
aug-cc-pVTZ EOM-CCSD	−379.268111	2108	894	786	5.41	125.5	122.2
cc-pVQZ EOM-CCSD	−379.284580	2114	914	791	5.46	126.1	122.8
cc-pVTZ EOM-CCSDT-3	−379.282456	2024	832	736	5.14	125.8	122.3
aug-cc-pVTZ EOM-CCSDT-3	−379.288674	2030	832	733	5.14	125.0	121.6
cc-pVQZ EOM-CCSDT-3	−379.306055	2030	854	735	5.17	125.6	122.2
cc-pVTZ EOM-CC3	−379.284939	2003	813	724	5.06	125.6	122.1
aug-cc-pVTZ EOM-CC3	−379.291267	2009	813	721	5.06	124.8	121.4
cc-pVQZ EOM-CC3	−379.308609	2008	837	722	5.10	125.5	122.0
MRCI/aug-cc-pVDZ (Ref.. 41)						130	

2.5.2.8 Lowest $^1\Delta$ state of HPC

The final state characterized in this study occurs for linear HPC. The excitation for this HPC $^1\Delta$ state is T_e=176.5 kcal mol^{-1}. Clearly, this electronic state is so far above the $H(^2S)+CP(X\ ^2\Sigma^+)$ dissociation limit to make observation unlikely. The excitation energy of this state relative to $^1\Sigma^+$ HPC is similar to T_e for $^1\Delta$ HCP (99.2 kcal mol^{-1} vs. 112.3 kcal mol^{-1}). The bond lengths for this state are remarkably similar to the bond lengths for the $^1\Sigma^-$ state of HPC.

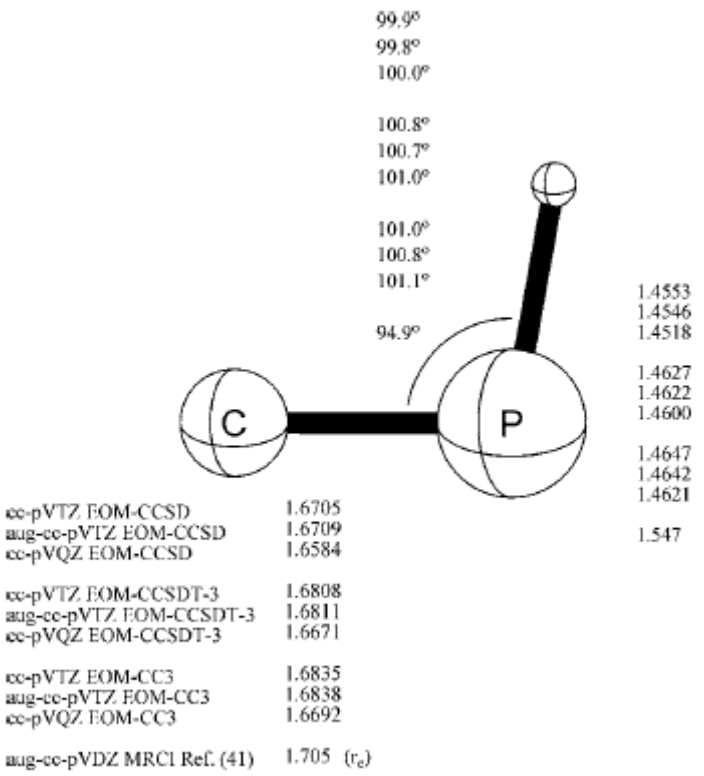

Figure 2.6: Predicted geometries of the $2\ ^1A'(^1\Delta)$ state of HPC. Bond lengths are in Å.

Table 2.11: Total energies (in hartree), bond lengths (in Å), and T_e (in kcal mol^{-1}) for the linear $1\ ^1\Delta$ state of HPC.

Level of theory	Total energy	*Re*_HP_	*Re*_CP_	*Te*
cc-pVTZ EOM-CCSD	−379.171918	1.4018	1.7784	183.1
aug-cc-pVTZ EOM-CCSD	−379.178807	1.4039	1.7736	181.5
cc-pVQZ EOM-CCSD	−379.193158	1.4010	1.7659	183.5
cc-pVTZ EOM-CCSDT-3	−379.199866	1.4107	1.8120	177.6
aug-cc-pVTZ EOM-CCSDT-3	−379.207597	1.4129	1.8075	175.9
cc-pVQZ EOM-CCSDT-3	−379.222941	1.4101	1.7987	177.8
cc-pVTZ EOM-CC3	−379.204264	1.4137	1.8230	176.3
aug-cc-pVTZ EOM-CC3	−379.212126	1.4161	1.8186	174.5
cc-pVQZ EOM-CC3	−379.227389	1.4131	1.8091	176.5

2.6 Conclusions

Ten stationary points on the ground and excited singlet state potential energy surfaces of HCP have been characterized. It is confirmed that linear HCP is the only genuine minimum on the ground state surface, with the other stationary point, linear HPC, serving as a stationary point of Hessian index 2. The physical properties determined for linear HCP compare favorably with the available experimental observations. The cc-pV5Z CCSD(T) vibrational frequencies (ω_e) with experimental values[6] (ν_0) in parentheses are 3344 cm^{-1} (3217), 1298 cm^{-1} (1278), and 689 cm^{-1} (675) and the electric dipole moment at the cc-pVQZ CCSD level of theory is 0.373 D [0.390 (Ref. 2)]. The dissociation energy $\left[HCP\left(\widetilde{X}\ ^1\Sigma^+\right)\rightarrow H\left(^2S\right)+CP\left(X\ ^2\Sigma^+\right)\right]$ is predicted to be 119.0 kcal mol^{-1} which agrees well with the experimentally estimated value of 119.1 kcal mol^{-1}. Eight excited singlet electronic states including four linear stationary points and four bent minimum were considered. The energetic ordering of these states with respect to ground state $\widetilde{X}\ ^1\Sigma^+$ HCP (in kcal mol^{-1}) is

$$\widetilde{X}\ ^1\Sigma^+(HCP,0.0)<\widetilde{X}\ ^1\Sigma^+(HPC,78.6)<{}^1A''(HCP,101.4)<{}^1\Sigma^-(HCP,104.6)<{}^1A'(HCP,111.2)$$
$$<{}^1\Delta(HCP,112.4)<{}^1A''(HPC,122.3)<{}^1A'(HPC,125.6)<{}^1\Sigma^-(HPC,171.6)<{}^1\Delta(HPC,177.8)$$

These are the most definitive theoretical results reported to date for the important HCP/HPC system. The present predictions for the lowest $^1A''$ state of HCP compare favorably with the experimental results of Johns *et al.*[6] For the experimentally reported $\widetilde{C}\ ^1A'$ state, the agreement between theory and experiment leaves much to be desired.

2.7 Acknowledgment

This research was supported by the National Science Foundation Grant No. CHE-0451445.

2.8 References

[1]T. E. Gier, J. Am. Chem. Soc. **83**, 1769 (1961).

[2]J. K. Tyler, J. Chem. Phys. **40**, 1170 (1964).

[3] J. A. Kaye and D. F. Strobel, Icarus **59**, 314 (1984).

[4]B. E. Turner, T. Tsuji, J. Bally, M. Guelin, and J. Cernicharo, Astrophys. J. **365**, 569 (1990).

[5]D. D. S. MacKay and S. B. Charnley, Mon. Not. R. Astron. Soc. **325**, 545 (2001).

[6]J. W. C. Johns, H. F. Shurvell, and J. K. Tyler, Can. J. Phys. **47**, 893 (1969).

[7]J. G. Moehlmann, A. Hartford, and J. R. Lombardi, Can. J. Phys. **50**, 1705 (1972).

[8]D. C. Frost, S. T. Lee, and C. A. McDowell, Chem. Phys. Lett. **23**, 472 (1973).

[9]H. Ishikawa, C. Nagao, and N. Mikami, J. Mol. Spectrosc. **194**, 52 (1999).

[10]J. M. Garneau and A. Cabana, J. Mol. Spectrosc. **69**, 319 (1978).

[11]J. M. Garneau and A. Cabana, J. Mol. Spectrosc. **79**, 502 (1980).

[12]J. M. Garneau and A. Cabana, J. Mol. Spectrosc. **87**, 490 (1981).

[13]A. Cabana, Y. Doucet, J. M. Garneau, C. Pepin, and P. Puget, J. Mol. Spectrosc. **96**, 342 (1982).

[14]V. F. Kalasinsky and S. Pechsiri, J. Raman Spectrosc. **16**, 190 (1985).

[15]M. A. Mason and K. K. Lehmann, J. Chem. Phys. **98**, 5184 (1993).

[16] G. Strey and I. M. Mills, Mol. Phys. **26**, 129 (1973).

[17]P. Dréan, J. Demaison, L. Poteau, and J. M. Denis, J. Mol. Spectrosc. **176**, 139 (1996).

[18]H. Ishikawa, H. Toyosaki, N. Mikami, F. Perez-Bernal, P. H. Vaccaro, and F. Iachello, Chem. Phys. Lett. **365**, 57 (2002).

[19]A. Ruoff and W. Sawodny, J. Mol. Spectrosc. **33**, 556 (1970).

[20]H. F. Shurvell, J. Phys. Chem. **74**, 4257 (1970).

[21]J. B. Robert, H. Marsmann, I. Absar, and J. R. Van Wazer, J. Am. Chem. Soc. **93**, 3320 (1971).

[22]G. F. Adams, J. Mol. Struct. **9**, 190 (1971).

[23]N. Mohan and A. Muller, J. Mol. Struct. **12**, 275 (1972).

[24]C. Thomson, Theor. Chim. Acta **35**, 237 (1974).

[25]J. F. Ogilvie, Can. J. Spectrosc. **19**, 171 (1974).

[26]J. B. Collins, P. R. Schleyer, J. S. Binkley, and J. A. Pople, J. Chem. Phys. **64**, 5142 (1976).

[27]C. Thomson and P. Ellam, Theor. Chim. Acta **62**, 62 (1982).

[28]P. Botschwina, Chem. Phys. **81**, 73 (1983).

[29]J. E. Bloor and J. G. Yu, J. Phys. Chem. **94**, 5586 (1990).

[30]S. M. Bachrach, J. Comput. Chem. **10**, 392 (1989).

[31]L. L. Lohr, J. Mol. Spectrosc. **162**, 300 (1993).

[32]P. K. Chattaraj, S. Nath, and A. B. Sannigrahi, J. Phys. Chem. **98**, 9143 (1994).

[33]S. C. Farantos, H. M. Keller, R. Schinke, K. Yamashita, and K. Morokuma, J. Chem. Phys. **104**, 10055 (1996).

[34]C. Puzzarini, R. Tarroni, P. Palmieri, J. Demaison, and M. L. Senent, J. Chem. Phys. **105**, 3132 (1996).

[35]J. K. G. Watson, Chem. Phys. **283**, 171 (2002).

[36]C. Puzzarini, Phys. Chem. Chem. Phys. **6**, 344 (2004).

[37]J. E. Del Bene, J. Elguero, and I. Alkorta, J. Phys. Chem. A **108**, 3662 (2004).

[38]A. Dransfeld, Chem. Phys. **298**, 47 (2004).

[39]S. P. Karna, P. J. Bruna, and F. Grein, Can. J. Phys. **68**, 499 (1990).

[40]A. B. Sannigrahi and F. Grein, Chem. Phys. Lett. **214**, 609 (1993).

[41]S. Nanbu, S. K. Gray, T. Kinoshita, and M. Aoyagi, J. Chem. Phys. **112**, 5866 (2000).

[42]E. S. Goldstein, S. Q. Jin, M. R. Carrillo, and R. J. Cave, J. Comput. Chem. **14**, 186 (1993).

[43]K. K. Lehmann, S. C. Ross, and L. L. Lohr, J. Chem. Phys. **82**, 4460 (1985).

[44]N. L. Ma, S. S. Wong, M. N. Paddon-Row, and W. K. Li, Chem. Phys. Lett. **213**, 189 (1993).

[45]H. S. Hong and R. J. Cave, J. Phys. Chem. **98**, 10036 (1994).

[46]C. Beck, R. Schinke, and J. Koput, J. Chem. Phys. **112**, 8446 (2000).

[47]H. Ishikawa, R. W. Field, S. C. Farantos, M. Joyeux, J. Koput, C. Beck, and R. Schinke, Annu. Rev. Phys. Chem. **50**, 443 (1999).

[48]T. H. Dunning, J. Chem. Phys. **90**, 1007 (1989).

[49]R. A. Kendall, T. H. Dunning, and R. J. Harrison, J. Chem. Phys. **96**, 6796 (1992).

[50]D. E. Woon and T. H. Dunning, J. Chem. Phys. **98**, 1358 (1993).

[51]G. D. Purvis and R. J. Bartlett, J. Chem. Phys. **76**, 1910 (1982).

[52]M. Rittby and R. J. Bartlett, J. Phys. Chem. **92**, 3033 (1988).

[53]K. Raghavachari, G. W. Trucks, J. A. Pople, and M. Head-Gordon, Chem. Phys. Lett. **157**, 479 (1989).

[54]G. E. Scuseria, Chem. Phys. Lett. **176**, 27 (1991).

[55]J. Noga, R. J. Bartlett, and M. Urban, Chem. Phys. Lett. **134**, 126 (1987).

[56]H. Koch, O. Christiansen, P. Jørgensen, A. M. S. de Meras, and T. Helgaker, J. Chem. Phys. **106**, 1808 (1997).

[57]D. C. Comeau and R. J. Bartlett, Chem. Phys. Lett. **207**, 414 (1993).

[58]J. F. Stanton and R. J. Bartlett, J. Chem. Phys. **98**, 7029 (1993).

[59]J. F. Stanton, J. Gauss, W. J. Lauderdale, J. D. Watts, and R. J. Bartlett, ACESII. This package also contains modified versions of the MOLECULE Gaussian integral program of J. Almlof and P. R. Taylor, the ABACUS integral derivative program written by T. U. Helgaker, H. J. Aa. Jorgensen, and P. R. Taylor, and the PROPS property evaluation code of P. R. Taylor.

[60]H.-J. Werner, P. J. Knowles, R. D. Ramos *et al.*, MOLPRO, a package of *ab initio* programs designed, version 2002.1.

[61]R. M. Badger, J. Chem. Phys. **2**, 128 (1934).

[62]R. M. Badger, J. Chem. Phys. **3**, 710 (1934).

[63]A. D. Walsh, J. Chem. Soc. 2288 (1953).

CHAPTER 3

ISOLATION AND IDENTIFICATION OF UNUSUALLY STABLE TRIPLET CARBENES[2]

[2] J. B. Ingels, W. D. Allen, H. F. Schaefer III, and P. Schreiner. To be submitted to *J. Chem. Phys*.

3.1 Abstract

Perchlorosilylcarbene ($ClC\text{-}SiCl_3$) has been prepared experimentally and trapped in an argon matrix. Identification then occurs based on the IR spectrum and ESR signal of the molecule taken in the matrix. High accuracy *ab initio* methods are used in conjunction with focal-point extrapolations to definitively determine whether the trapped species is a singlet or triplet species. Our results show the triplet to be lower in energy than the singlet with regards to the perchlorosilylcarbene species. A vibrational analysis that includes anharmonic effects provides a means to compare to the IR spectra obtained experimentally. It was also found that the species formed upon isomerization, perchlorosilylethylene ($Cl_2C\text{-}SiCl_2$), is less stable than the perchlorosilylcarbene species.

3.2 Introduction

In a progression of joint experimental and theoretical ventures, stable triplet carbenes have been produced in a cold matrix (~11 K) and identified by both their IR and EPR spectra along with high-level theoretical predictions[1,2]. The first such species studied was ethylidene ($H\text{-}C\text{-}CH_3$), prepared by the reaction of SiH_4 and carbon atoms in the ^3P state. Schreiner and Reisenauer have published details of the experimental apparatus[3]. The experimentalists found an EPR signal with zero-field splitting parameters and a hyperfine structure that is consistent with a nearly linear H-C-Si moiety. Of course, with this data it can still be ambiguous as to whether the triplet carbene or triplet silyl ethylene structure is being generated. Theoretical predictions by Sattelmeyer and Allen found that indeed the triplet carbene lay lower in energy than singlet carbene species but still higher in energy than both singlet and triplet silylethylene species. A frequency analysis performed at the CCSD(T)/cc-pVTZ level of theory granted excellent agreement between the theoretical fundamental frequencies and the experimental fundamental frequencies (< 10 cm^{-1} and without empirical scaling) for the experimental species, including the parent and a deuterated analog. All other species were also optimized and frequency analysis carried out and significant agreement was not found with any of these species and the experimental vibrational frequencies.

The next step in the progression was the generation and characterization of the analogous dichloro triplet carbene (H-C-$SiHCl_2$)[1]. This dichloro signal was prepared in a similar manner to the parent species mentioned above and also produced an EPR signal that confirms the spin state to be a triplet. From a theoretical standpoint the species were again optimized at the CCSD(T)/cc-pVTZ level of theory and excellent agreement was found between the theoretically predicted fundamental frequencies and the experimentally determined fundamental frequencies. The triplet carbene species was predicted to lie 18 kcal mol^{-1} below the singlet carbene but again 20-40 kcal mol^{-1} above the triplet and singlet silylethylene species. An interesting note, in most studies of carbene species the open-shell singlet state is completely neglected. In this case, DFT found that the open-shell species lie very close to the triplet species and hence could play a role in the chemistry of the species. However, more rigorous *ab initio* techniques found the open-shell species to lie roughly 28 kcal mol^{-1} above the triplet carbene species, ending that argument.

In the present study, the perchloro carbene (Cl-C-$SiCl_3$) species was studied to finish out the progression and again aid in experimental characterization. The potential energy surface was predicted at the CCSD(T)/cc-pVTZ level of theory for the six stationary points found on the singlet and triplet surfaces. To further nail down the energetics, focal-point analysis (FPA) is carried out to extrapolate to the complete basis set (CBS) limit. A frequency analysis was incorporated, including anharmonic corrections to nail down experimental IR assignment and total energy distributions (TED). These results will be compared with the experimental data to evaluate the nature of the isolated species.

3.3 Computational Details

Electronic energies, optimized geometries, and vibrational frequencies were determined for six species on the singlet and triplet potential surfaces for the perchloro species. The basis sets utilized in this study are the correlation consistent basis sets (cc-pVXZ where X=T,Q,5) of Dunning and co-workers[4,5]. The basis set used for optimization and frequency analysis, cc-pVTZ consisted of 200 contracted Gaussian functions. The zeroth-order description of the stationary points was obtained using restricted Hartree-Fock (RHF) for the singlets and restricted open-shell Hartree-Fock (ROHF) for the triplets. The

stationary points on the potential surface were optimized at the MP2, CCSD[6,7], and CCSD(T)[8-10] levels of theory. The ZAPT2 method was used in place of MP2 for the single-point triplet calculations due to better implementation in MPQC that led to greater accessibility of the calculations with a larger basis set. Core orbitals frozen in the computation include the 1*s*-like orbital of carbon and the 1*s*-, 2*s*-, and 2*p*-like orbitals of phosphorus. Computational packages utilized in this work include ACESII (Ref. 11), MOLPRO[12], and MPQC[13].

3.4 Results

In Figure 2.1 the stationary points optimized in this study are schematically depicted showing energy differences determined with the MP2/cc-pVTZ level of theory with complete basis set (CBS) extrapolations applied. Relative energy differences between the stationary points at both the MP2/cc-pVTZ and CCSD(T) CBS limit are tabulated in Tables 3.1 and 3.7, respectively. FPA tables can be found in Tables 3.2 to 3.6. Compiled information on vibrational analysis and TED for each of the stationary points are shown in Tables 3.8 to 3.13. Cartesian coordinates, description of internal coordinates, quadratic force fields, and single point energies used in the FPA can be found in Tables 3.14 to 3.17, respectively.

3.4.1 Potential Energy Surface

The six stationary points on the potential energy surface are depicted schematically in Figure 2.1. Note that the relative energies are found by a focal-point analysis to the CBS limit using the MP2/cc-pVTZ geometry as the reference. There are two surfaces present, the singlet and the triplet, depicting a reactant silylcarbene, product silylethylene, and a transition state for the triplet state only. It is important to note here that ^{3}**1** is the global minimum on the surface making it different than the previous two studies of the parent and dichloro species. In fact, this may be the only known chemical species to show an energetic preference for the triplet carbene over the ethylene species[14]. The same relative ordering, on a given side, as the previous two studies was held for the perchloro species, the triplet carbene was lower than the singlet carbene and the singlet ethylene lower than the triplet ethylene. Table 3.1 shows the various relative energy differences at the CCSD(T) CBS limit with the MP2/cc-pVTZ reference geometry.

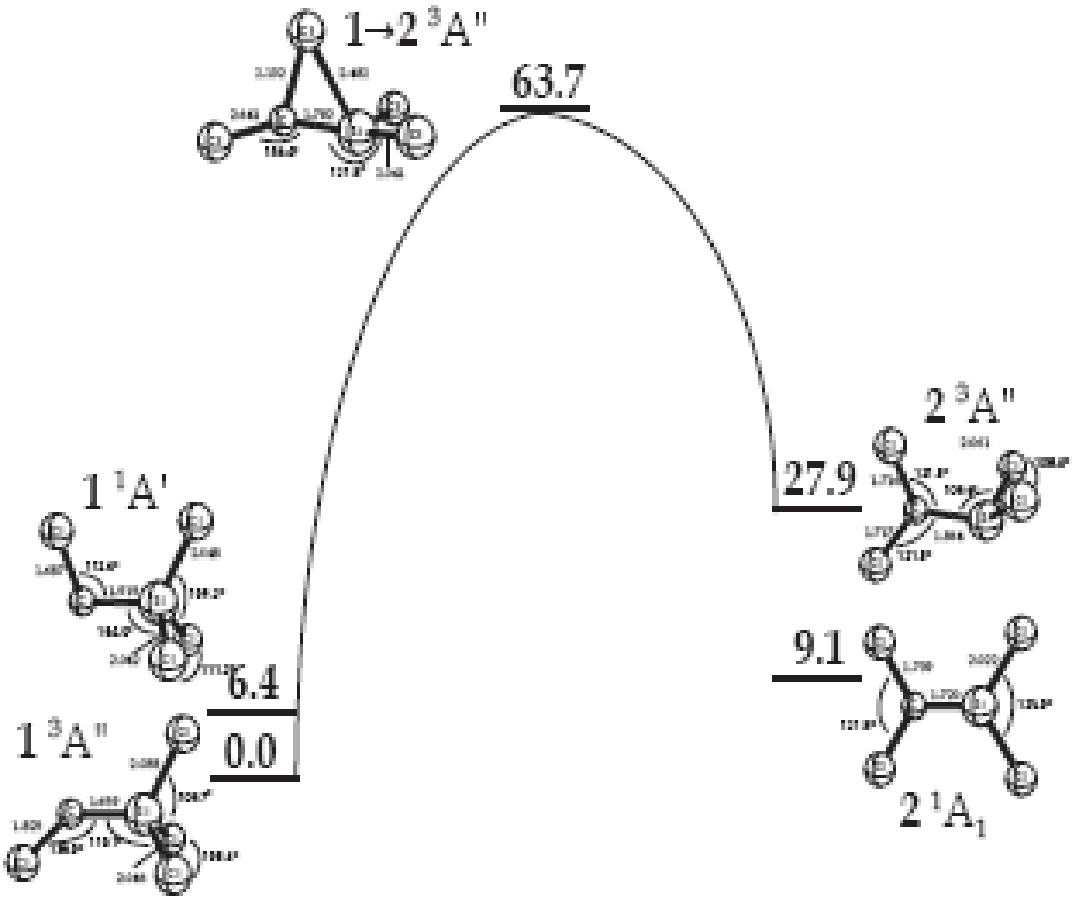

Figure 3.1: Potential energy surface depicting the full triplet surface and showing relative energies of two singlet species. Relative energies shown are CCSD(T) CBS limit with MP2/cc-pVTZ reference geometry (in kcal mol^{-1}). Bond lengths and angles are at the CCSD(T)/cc-pVTZ reference geometry.

Table 3.1: Relative energy table (in kcal mol^{-1}) for all six stationary points. Energetic values represent the difference in energy at the MP2/cc-pVTZ level of theory of the species at the top minus the species on the left.

	^{3}**1**	^{1}**2**	^{1}**1**	^{3}**2**	^{1}**1**→**2**	^{3}**1**→**2**
^{3}**1**	0.0					
^{1}**2**	5.6	0.0				
^{1}**1**	9.6	4.0	0.0			
^{3}**2**	24.7	19.2	15.1	0.0		
^{1}**1**→**2**	34.4	28.8	24.8	9.6	0.0	
^{3}**1**→**2**	63.5	58.0	54.0	38.8	29.2	0.0

3.4.2 Focal-Point Analysis

The focal-point analysis (FPA) was carried out using the prescription outlined by Császár, Allen, and Schaefer[15]. The reference geometry used was the optimized MP2/cc-pVTZ geometry. Single point energies are then calculated for each species at this geometry using the SCF, MP2/ZAPT2, CCSD, and CCSD(T) methods (MP2 used for singlet species, ZAPT2 used for triplet species, ZAPT2 is equivalent to MP2 for closed-shell species). Basis sets used in conjunction with the above methods are the cc-pVXZ (X=T,Q,5) series. The largest basis set used for each of the methods was cc-pV5Z except for CCSD(T) where cc-pVQZ was the largest basis set used. The energies for each method in the table are reported as corrections to the method immediately to its left. Each method is independently extrapolated to the CBS limit (E_∞) and the final corrections summed across the table to determine an E_∞ for CCSD(T). The extrapolation scheme used for SCF is

$$E_\infty = E - be^{-cX}$$

with the three unknowns E_∞, b, and c means that the three energies at the highest level of theory are used for extrapolation and the X stands for the cardinal number of the basis set (e.g. 3 for cc-pVTZ, 4 for cc-pVTZ, and 5 for cc-pV5Z)[16]. The extrapolation scheme used for the post-SCF methods [MP2/ZAPT2, CCSD, and CCSD(T)] is

$$E_\infty = E - \frac{b}{X^3}$$

where only two unknowns E_∞ and b means that the two energies at the highest level of theory are used for extrapolation the X again stands for the cardinal number of the basis set[17].

The focal-point extrapolation for the two lowest lying species is shown in Table 3.2. The extrapolated energy difference of 9.119 kcal mol^{-1} widens the relative energy difference before extrapolation by nearly 4 kcal mol^{-1}, cementing the ^{3}**1** claim to the global minimum.

Table 3.2: Focal-point extrapolation for ^{1}**2** - ^{3}**1**.

^{1}**2** - ^{3}**1**	ΔE_e(HF)	+δ(MP2/ZAPT2)	+δ(CCSD)	+δ[CCSD(T)]	= E_e[CCSD(T)]
cc-pVTZ	38.696	-36.332	10.703	-3.456	8.961
cc-pVQZ	38.652	-37.005	11.549	-4.106	8.957
cc-pV5Z	38.710	-37.046	11.812	[-4.240]	[9.029]
∞	[38.786]	[-37.088]	[12.087]	[-4.655]	**[9.119]**
Function	$a+be^{-cX}$	$a+bX^{-3}$	$a+bX^{-3}$	$a+bX^{-3}$	
Fit pts., X =	(3,4,5)	(4,5)	(4,5)	(3,4)	

The focal-point extrapolation for the two silylcarbene species is shown in Table 3.3. The extrapolated energy difference of 6.383 kcal mol^{-1} narrows the relative energy difference before extrapolation by more than 3 kcal mol^{-1}, swapping the relative energy ordering of the two singlet minima.

Table 3.3: Focal point extrapolation for ^{1}**1** - ^{3}**1**.

^{1}**1** - ^{3}**1**	ΔE_e(HF)	+δ(MP2/ZAPT2)	+δ(CCSD)	+δ[CCSD(T)]	= E_e[CCSD(T)]
cc-pVTZ	23.318	-16.931	2.968	-2.330	7.026
cc-pVQZ	23.386	-17.950	3.583	-2.426	6.593
cc-pV5Z	23.465	-18.367	3.855	[-2.459]	[6.494]
∞	[23.541]	[-18.805]	[4.141]	[-2.493]	**[6.383]**
Function	$a+be^{-cX}$	$a+bX^{-3}$	$a+bX^{-3}$	$a+bX^{-3}$	
Fit pts., X =	(3,4,5)	(4,5)	(4,5)	(3,4)	

The focal point extrapolation for the two silylethylene species is shown in Table 3.4. The relative energy difference of 18.793 kcal mol^{-1} which changes little from relative energy before extrapolation (~0.4 kcal mol^{-1}). When combined with the extrapolation between ^{1}**2** and ^{3}**1**, the relative energy difference for the ^{3}2 and the global minimum is 27.912 kcal mol^{-1}.

Table 3.4: Focal point extrapolation for ^{3}**2** - ^{1}**2**.

^{3}**2** - ^{1}**2**	ΔE_e(HF)	+δ(MP2/ZAPT2)	+δ(CCSD)	+δ[CCSD(T)]	= E_e[CCSD(T)]
cc-pVTZ	-3.774	25.507	-7.043	2.669	16.998
cc-pVQZ	-3.323	26.409	-7.907	2.739	17.918
cc-pV5Z	-3.026	26.634	-8.125	[2.899]	[18.382]
∞	[-2.790]	[26.870]	[-8.355]	[3.067]	**[18.793]**
Function	$a+be^{-cX}$	$a+bX^{-3}$	$a+bX^{-3}$	$a+bX^{-3}$	
Fit pts., X =	(3,4,5)	(4,5)	(4,5)	(3,4)	

The focal point extrapolation for the triplet transition state and the triplet carbene is shown in Table 3.5. The relative energy difference (barrier to chlorine rearrangement) of 63.672 kcal mol^{-1} is roughly the same as that of the relative energy before extrapolation.

Table 3.5: Focal point extrapolation for ^{3}**TS** - ^{3}**1**.

^{3}**TS** - ^{3}**1**	ΔE_e(HF)	+δ(MP2/ZAPT2)	+δ(CCSD)	+δ[CCSD(T)]	= E_e[CCSD(T)]
cc-pVTZ	83.678	-20.348	3.615	-4.784	62.161
cc-pVQZ	83.868	-20.103	4.109	-5.006	62.869
cc-pV5Z	84.087	-19.924	4.190	[-5.081]	[63.272]
∞	[84.294]	[-19.737]	[4.275]	[-5.115]	**[63.672]**
Function	$a+be^{-cX}$	$a+bX^{-3}$	$a+bX^{-3}$	$a+bX^{-3}$	
Fit pts., X =	(3,4,5)	(4,5)	(4,5)	(3,4)	

The focal point extrapolation for the singlet transition state and the singlet carbene is shown in Table 3.6. The relative energy difference (barrier to chlorine rearrangement) of 29.748 kcal mol^{-1} raises the barrier

by 5 kcal mol^{-1}, however, this barrier is still considerably less than the barrier to rearrangement on the triplet surface.

Table 3.6: Focal point extrapolation for 1**TS** - ^{1}**1**.

^{1}**TS** - ^{1}**1**	ΔE_e(HF)	+δ(MP2/ZAPT2)	+δ(CCSD)	+δ[CCSD(T)]	= E_e[CCSD(T)]
cc-pVTZ	44.289	-19.517	7.527	-2.715	29.584
cc-pVQZ	44.260	-19.643	7.917	-2.865	29.669
cc-pV5Z	44.255	-19.602	7.987	[-2.935]	[29.705]
∞	[44.256]	[-19.559]	[8.059]	[-3.008]	**[29.748]**
Function	$a+be^{-cX}$	$a+bX^{-3}$	$a+bX^{-3}$	$a+bX^{-3}$	
Fit pts., X =	(3,4,5)	(4,5)	(4,5)	(3,4)	

Table 3.7: Relative energy table (in kcal mol^{-1}) for all six stationary points. Represents the difference in energy at the CCSD(T) CBS limit (with a MP2/cc-pVTZ reference geometry) level of theory of the species on the left minus the species at the top.

	^{3}**1**	^{1}**1**	^{1}**2**	^{3}**2**	^{1}**1→2**	^{3}**1→2**
^{3}**1**	0.0					
^{1}**1**	6.4	0.0				
^{1}**2**	9.2	2.7	0.0			
^{3}**2**	27.9	21.5	18.8	0.0		
^{1}**1→2**	36.1	29.7	27.0	8.2	0.0	
^{3}**1→2**	63.7	57.3	54.6	35.8	33.9	0.0

3.4.3 Vibrational Analysis

The vibrational analysis was carried out for each stationary point, at each optimized geometry. These vibrational frequencies are determined using equilibrium geometries as the reference and are harmonic (ω) rather than fundamental (ν) frequencies. One must take care when comparing these predicted frequencies to experimentally derived frequencies. Included with each of the set of frequencies are total energy distributions (TED) which give for each normal mode the relative contribution of each of the

symmetry adapted internal coordinates. The TED were determined using an in-house FORTRAN based program INTDER[18,19].

For the ^{3}**1** species the vibrational frequencies at all levels of theory and the TED are shown in Table 3.8. Three intense peaks are expected in the IR spectrum in the range of 603 to 626 cm^{-1}, these three peaks consist primarily of chlorine stretches and the C-Si stretch. For the ^{1}**1** species, the vibrational frequencies at each level of theory are summarized in Table 3.9. Note the similar structure to its corresponding triplet with the exception of the *cis* nature of the chlorine atom connected to the carbon atom (see Figure 2.1). The vibrational frequencies are also similar with three intense peaks expected in a similar range, with each intense peak 10 to 20 cm^{-1} higher in energy. Table 3.10 summarizes the vibrational frequencies for the ^{3}**2** species and shows three intense peaks, two in a similar range to the aforementioned species and one 300 cm^{-1} higher in energy. The vibrational frequencies of ^{1}**2** are summarized in Table 3.11, again three intense peaks though one is roughly one-fourth the intensity of the others. Similar to the ^{3}**2** species, two of the peaks should appear in the same range as the two silylcarbene species while the other appears 300 cm^{-1} higher in energy. The triplet transition state is summarized in Table 3.12, note the imaginary frequency at the bottom of the table, as required for a species to be a transition state. The TED for the transition state reveals the motion that would be expected in this case. The C-Cl distance would decrease as the Si-Cl distance would increase (and vice-versa) as would the opposite phase movement of the Cl-C-Si and the Si-Cl-C angles.

The experimentally derived difference IR spectrum found by Schreiner and co-workers is shown in Figure 2.2[14]. Most notable are the three intense peaks found at roughly 598, 601, and 615 cm^{-1}. The vibrational analysis of each of the four minima on the PES shown that 2 or 3 intense peaks were expected within 50 cm^{-1} of that range for each species. The anharmonic corrections to our predicted frequencies is not expected to be large, mostly since there are no hydrogen stretches involved. Assuming 10 cm^{-1} or

Table 3.8: Vibrational analysis of ^{3}**1**. IR intensities in (km mol^{-1}) and TED based on MP2/cc-pVTZ geometry (only contributions greater than 5 shown). All the methods executed using a cc-pVTZ basis set.

Mode	MP2	CCSD	CCSD(T)	Total Energy Distribution (TED)
$\omega_1(a')$	1144(10)	1129	1117	CCl str (59) – CSi str (40)
$\omega_2(a')$	634(186)	631	626	$SiCl_3$ asym str (91)
$\omega_9(a'')$	615(188)	613	607	$SiCl_3$ asym str (95)
$\omega_3(a')$	605(191)	608	603	CSi str (42) + CCl str (32) – $SiCl_3$ sym str (19)
$\omega_4(a')$	448(2)	448	443	$SiCl_3$ sym str (70) CSi str (15) + CSi str (5)
$\omega_5(a')$	297(9)	299	295	SiCCl bend(30) + $SiCl_3$ tilt (28) + $SiCl_3$ umbrella (21) + $SiCl_3$ sym str (8)
$\omega_{10}(a'')$	266(11)	267	263	$SiCl_2$ twist (78) + $SiCl_2$ rock (10) – $SiCl_3$ internal rotation (8)
$\omega_6(a')$	212(6)	213	211	$SiCl_3$ umbrella (61) + $SiCl_2$ scissor (21) – $SiCl_3$ tilt (9)
$\omega_{11}(a'')$	170(0.5)	170	168	$SiCl_2$ rock (86) – $SiCl_2$ twist (7) + $SiCl_3$ internal rotation (6)
$\omega_7(a')$	161(1)	163	161	$SiCl_2$ scissor (70) + SiCCl bend (10) - $SiCl_3$ umbrella (10) + $SiCl_3$ tilt (9)
$\omega_8(a')$	78(1)	81	79	SiCCl bend (58) – $SiCl_3$ tilt (40)
$\omega_{12}(a'')$	34(0.1)	36	35	$SiCl_3$ internal rotation (86) + $SiCl_2$ twist (12)

Table 3.9: Vibrational analysis of ^{1}**1**. IR intensities in (km mol^{-1}) and TED based on MP2/cc-pVTZ geometry (only contributions greater than 5 shown). All the methods executed using a cc-pVTZ basis set.

Mode	MP2	CCSD	CCSD(T)	Total Energy Distribution (TED)
$\omega_1(a')$	965(47)	943	920	CCl str (76) – CSi str (24)
$\omega_2(a')$	656(103)	648	642	CSi str (54) + CCl str (22) – $SiCl_3$ sym str (11)
$\omega_9(a'')$	628(191)	623	616	$SiCl_3$ asym str (97)
$\omega_3(a')$	619(176)	614	608	$SiCl_3$ asym str (86)
$\omega_4(a')$	454(18)	451	445	$SiCl_3$ sym str (74) + CSi str (10) – SiCCl bend (10)
$\omega_5(a')$	304(6)	302	298	SiCCl bend(41) + $SiCl_3$ umbrella (21) - $SiCl_3$ tilt(17) + $SiCl_3$ sym str (11)
$\omega_{10}(a'')$	234(24)	235	228	$SiCl_2$ twist (70) – $SiCl_3$ internal rotation (17) + $SiCl_2$ rock (11)
$\omega_6(a')$	207(5)	208	205	$SiCl_3$ umbrella (55) - $SiCl_2$ scissor (26) + $SiCl_3$ tilt (10) – CSi str (5)
$\omega_{11}(a'')$	172(0.1)	172	169	$SiCl_2$ rock (87) – $SiCl_2$ twist (8) + $SiCl_3$ internal rotation (5)
$\omega_7(a')$	158(3)	159	156	$SiCl_2$ scissor (60) - SiCCl bend (20) + $SiCl_3$ umbrella (17)
$\omega_8(a')$	101(0.9)	102	100	$SiCl_3$ tilt (66) + SiCCl bend (27) + $SiCl_2$ scissor (7)
$\omega_{12}(a'')$	23(0.3)	21	21	$SiCl_3$ internal rotation (78) + $SiCl_2$ twist (22)

Table 3.10: Vibrational analysis of ^{3}**2**. IR intensities in (km mol^{-1}) and TED based on MP2/cc-pVTZ geometry (only contributions greater than 5 shown). All the methods executed using a cc-pVTZ basis set.

Mode	MP2	Total Energy Distribution (TED)
$\omega_1(a')$	1008(4)	CSi str (50) – CCl_2 sym str (39) + CCl_2 bend (10)
$\omega_2(a')$	910(133)	CCl_2 asym str (97)
$\omega_9(a'')$	595(177)	$SiCl_2$ asym str (97)
$\omega_3(a')$	547(111)	$SiCl_2$ sym str (76) – CCl_2 sym str (13) – CSi str (6)
$\omega_4(a')$	446(22)	CCl_2 sym str (40) + CSi str (16) + $SiCl_2$ sym str (39) – $SiCl_2$ twist (10)
$\omega_5(a')$	308(13)	CCl_2 bend (42) + $SiCl_2$ twist (36) – CCl_2 rock (11) + CCl_2 sym str (5)
$\omega_{10}(a'')$	295(4)	CCl_2 twist (50) – $SiCl_2$ rock (43)
$\omega_6(a')$	244(3)	CCl_2 bend (36) – $SiCl_2$ twist (22) + CCl_2 rock (15) – $SiCl_2$ twist (9)
$\omega_7(a')$	155(2)	$SiCl_2$ bend (73) + CCl_2 rock (10) + CCl_2 bend (7) – $SiCl_2$ twist (5)
$\omega_8(a')$	104(0.9)	CCl2 rock (59) + SiCl2 twist (37)
$\omega_{11}(a'')$	87(0.1)	SiCl2 rock (53) + CCl2 twist (48)
$\omega_{12}(a'')$	14(0.1)	CSi internal rotation (97)

Table 3.11: Vibrational analysis of ^{1}**2**. IR intensities in (km mol^{-1}) and TED based on MP2/cc-pVTZ geometry (only contributions greater than 5 shown). All the methods executed using a cc-pVTZ basis set.

Mode	MP2	CCSD	CCSD(T)	Total Energy Distribution (TED)
$\omega_1(a_1)$	1169 (7)	1193	1157	CSi str (70) – CCl_2 sym str (21) + CCl_2 bend (7)
$\omega_9(b_2)$	891 (42)	887	867	CCl_2 asym str (98)
$\omega_{10}(b_2)$	675 (154)	670	663	$SiCl_2$ asym str (94)
$\omega_2(a_1)$	608 (117)	605	595	$SiCl_2$ sym str (51) – CCl_2 sym str (37) – CSi str (6)
$\omega_3(a_1)$	410 (3)	408	400	CCl_2 sym str (40) + $SiCl_2$ sym str (39) + CSi str (16)
$\omega_7(b_1)$	280 (3)	285	268	CCl_2 twist (115) – $SiCl_2$ twist (-15)
$\omega_4(a_1)$	253 (1)	253	248	CCl_2 bend (73) – $SiCl_2$ bend (13) – $SiCl_2$ sym str (7)
$\omega_{11}(b_2)$	240 (4)	243	238	CCl_2 tilt (50) + $SiCl_2$ tilt (41) + $SiCl_2$ asym str (6)
$\omega_5(a_1)$	156 (0.8)	158	155	$SiCl_2$ bend (84) + CCl_2 bend (12)
$\omega_{12}(b_2)$	89 (1)	97	90	$SiCl_2$ rock (52) – CCl_2 rock (49)
$\omega_6(a_2)$	78 (0.0)	93	75	CSi internal rotation (100)
$\omega_8(b_1)$	67 (3)	77	55	$SiCl_2$ twist (115) – CCl_2 twist (15)

Table 3.12: Vibrational analysis of ^{1}**1**→**2**. IR intensities in (km mol^{-1}) and TED based on MP2/cc-pVTZ geometry (only contributions greater than 5 shown). All the methods executed using a cc-pVTZ basis set.

Mode	MP2	Total Energy Distribution (TED)
ω_1(a′)	1162 (244)	CCl str (59) – CSi str (48) – SiClC bend (-12)
ω_2(a′)	618 (190)	$SiCl_2$ asym str (96) – $SiCl_2$ rock (5)
ω_3(a″)	589 (168)	$SiCl_2$ sym str (59) – CCl str (21) + 12 (21) – CSi str (18)
ω_4(a′)	387 (61)	CSi str (35) – SiClC bend (27) + $SiCl_2$ sym str (15) + CCl str (11)
ω_5(a′)	278 (83)	12 (68) – $SiCl_2$ scissor (-31) + ClCSi bend (28) – $SiCl_2$ sym str (20)
ω_6(a′)	272 (7)	$SiCl_2$ tilt (59) + 10 (38)
ω_7(a″)	224 (3)	12 (71) – ClCSi bend (63) – $SiCl_2$ scissor (-39)
ω_8(a′)	142 (3)	$SiCl_2$ scissor (164) – 12 (-77) – ClCSi bend (7)
ω_9(a″)	139 (0.9)	$SiCl_2$ rock (106) + $SiCl_2$ tilt (-9)
ω_{10}(a′)	99 (51)	SiClC bend (74) + ClCSi bend (18) + CSi str (-13) + $SiCl_2$ scissor (9)
ω_{11}(a′)	32 (0.4)	Cl wag (60) – $SiCl_2$ tilt (51) – $SiCl_2$ rock (-11)
ω_{12}(a″)	981*i*	CCl/SiCl asym str (102) + ClCSi bend (-22) – SiClC bend (19) – CSi str (-12)

even 20 cm^{-1} as a ceiling to the corrections can work to immediately remove some of the minima. The ^{3}**2** species has just two intense peaks within range and one peak falls at 547 cm^{-1} which is unlikely to be corrected to near 598 cm^{-1}, even more so as the corrections are expected to be negative. The same can be assumed for the ^{1}**2** species with its 663 peak unlikely to be corrected within a few wavenumber of 615. That leaves the two silylcarbene species where the best fit would come from the triplet species as the singlet species has a 642 cm^{-1} frequency which is likely too large. Also the singlet species has one of its three peaks which is expected to be roughly half the intensity of the other two peaks, not consistent with the experimental spectrum.

To ensure the compatibility between the theoretical predictions for the 31 species and the experimental spectrum the anharmonic corrections were calculated at the CCSD(T)/cc-pVTZ level of theory. The corrections are revealed in Table 3.13 alongside the original theoretical harmonic vibrational frequencies from Table 3.8. To compare frequencies in this case, one finds 598 versus 594, 601 versus 601, and 615 versus 618 experimental vs. theoretical, respectively. This is excellent agreement to within 4 cm-1, within the assumptions made for comparisons in the previous two studies[1,2]. Note the corrections outside of ω_1 are less than 10 cm^{-1}, justifying the previous assumptions.

Table 3.13: Vibrational analysis of ^{3}**1** with anharmonic corrections.

Mode	CCSD(T)/ cc-pVTZ	Anharmonic Correction	Mode	CCSD(T)/ cc-pVTZ
$\omega_1(a')$	1117	-119	$\nu_1(a')$	998
$\omega_2(a')$	626	-8	$\nu_2(a')$	618
$\omega_9(a'')$	607	-6	$\nu_9(a'')$	601
$\omega_3(a')$	603	-9	$\nu_3(a')$	594
$\omega_4(a')$	443	-7	$\nu_4(a')$	436
$\omega_5(a')$	295	-5	$\nu_5(a')$	290
$\omega_{10}(a'')$	263	-4	$\nu_{10}(a'')$	259
$\omega_6(a')$	211	-2	$\nu_6(a')$	209
$\omega_{11}(a'')$	168	-1	$\nu_{11}(a'')$	167
$\omega_7(a')$	161	0	$\nu_7(a')$	161
$\omega_8(a')$	79	-1	$\nu_8(a')$	78
$\omega_{12}(a'')$	35	-4	$\nu_{12}(a'')$	31

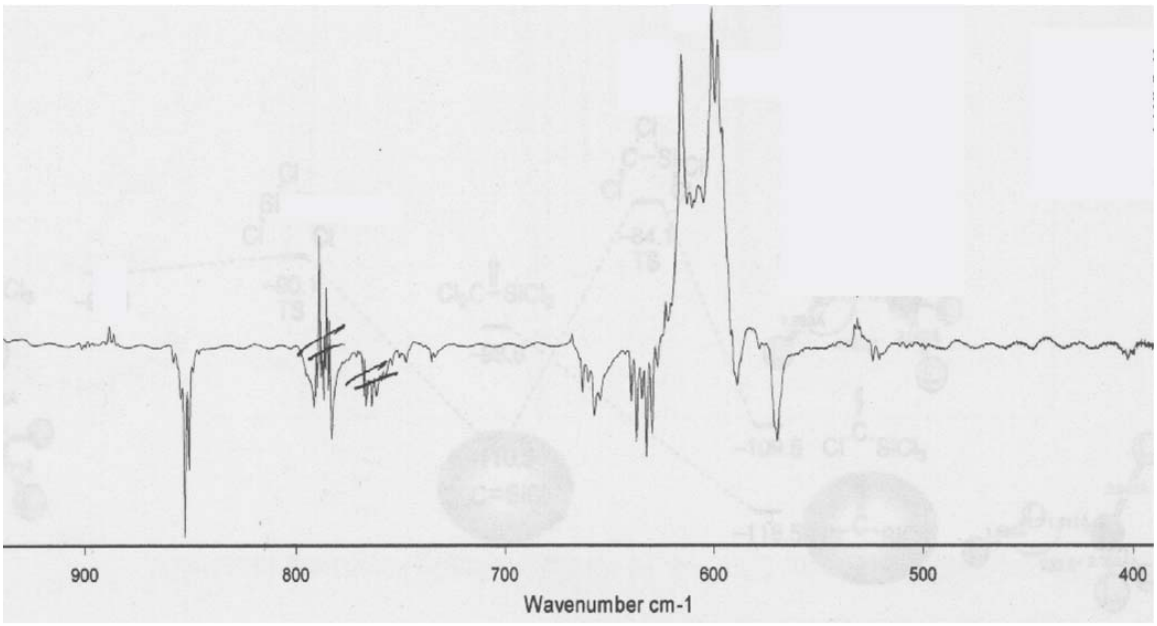

Figure 3.2: Difference IR spectrum found by Schreiner and co-workers[14].

3.5 Conclusions

The global minimum was found to be the triplet silylcarbene (^{3}**1**) species a result contrary to previous studies. The vibrational analysis predicted that with anharmonic corrections to the theoretically

determined harmonic frequencies, that the ^{3}**1** moiety most closely reproduces the peaks on the spectrum. These two predictions would provide ample evidence that the species Schreiner and co-workers trapped in the cold matrix is most likely the ^{3}**1** species if they are ever able to obtain a signal in the EPR spectrum.

3.6 References

[1]P. R. Schreiner, H. P. Reisenauer, W. D. Allen, and K. W. Sattelmeyer, *Org. Lett.* **6**, 1163 (2004).

[2]P. R. Schreiner, H. P. Reisenauer, K. W. Sattelmeyer, and W. D. Allen, *J. Am. Chem. Soc.* **127**, 12156 (2005).

[3]P. R. Schreiner and H. P. Reisenauer, *ChemPhysChem* **7**, 880 (2006).

[4]T. H. Dunning, *J. Chem. Phys.* **90**, 1007 (1989).

[5]D. E. Woon and T. H. Dunning, *J. Chem. Phys.* **98**, 1358 (1993).

[6]G. D. Purvis and R. J. Bartlett, *J. Chem. Phys.* **76**, 1910 (1982).

[7]M. Rittby and R. J. Bartlett, *J. Phys. Chem.* **92**, 3033 (1988).

[8]K. Raghavachari, G. W. Trucks, J. A. Pople, and M. Head-Gordon, *Chem. Phys. Lett.* **157**, 479 (1989).

[9]G. E. Scuseria and T. J. Lee, *J. Chem. Phys.* **93**, 5851 (1990).

[10]G. E. Scuseria, *Chem. Phys. Lett.* **176**, 27 (1991).

[11]J. F. Stanton, J. Gauss, W. J. Lauderdale, J. D. Watts, and R. J. Bartlett, ACESII. This package also contains modified versions of the MOLECULE Gaussian integral program of J. Almlof and P. R. Taylor, the ABACUS integral derivative program written by T. U. Helgaker, H. J. Aa. Jorgensen, and P. R. Taylor, and the PROPS property evaluation code of P. R. Taylor.

[12]H.-J. Werner, P. J. Knowles, R. D. Ramos et al., MOLPRO, a package of ab initio programs designed, version 2002.1.

[13]The Massively Parallel Quantum Chemistry Program (MPQC), Version *2.3.1*, C. L. Janssen, I. B. Nielsen, M. L. Leininger, E. F. Valeev, E. T. Seidl, Sandia National Laboratories, Livermore, CA, USA, 2004.

[14]P. R. Schreiner communication. An article including the experimental results and theoretical results could appear in the future.

[15]A. G. Császár, W. D. Allen, H. F. Schaefer III, J. Chem. Phys. 108, 9751 (1998).

[16]D. Feller, J. Chem. Phys. 96, 6104 (1992).

[17]T. Helgaker, W. Klopper, H. Koch, and J. Noga, J. Chem. Phys. 106, 9639 (1997).

[18]INTDER2000 is a general program developed by Wesley D. Allen and co-workers which performs various vibrational analyses and higher-order nonlinear transformations among force field representations.

[19]W. D. Allen and A. G. Császár, *J. Chem. Phys.* **98**, 2983 (1993).

3.7 Appendix

Table 3.14: Cartesian coordinates for each stationary point (in bohr).

^{3}**1**	MP2/cc-pVTZ			CCSD/cc-pVTZ			CCSD(T)/cc-pVTZ		
	x	y	z	x	y	z	x	y	z
Cl	-1.6048	2.3998	0.0000	-1.6200	2.3936	0.0000	-1.6382	2.3903	0.0000
C	-0.1098	-0.6985	0.0000	-0.1092	-0.7030	0.0000	-0.1111	-0.7023	0.0000
Si	-0.6698	5.3628	0.0000	-0.6755	5.3806	0.0000	-0.6830	5.3770	0.0000
Cl	-2.8961	-3.3376	0.0000	-2.8917	-3.3573	0.0000	-2.8862	-3.3715	0.0000
Cl	2.1023	-1.1449	3.1231	2.1052	-1.1411	3.1306	2.1100	-1.1319	3.1345
Cl	2.1023	-1.1449	-3.1231	2.1052	-1.1411	-3.1306	2.1100	-1.1319	3.1345

^{3}**2**	MP2/cc-pVTZ			CCSD/cc-pVTZ			CCSD(T)/cc-pVTZ		
	x	y	z	x	y	z	x	y	z
C	-0.0653	-1.9085	0.0000	-0.0607	-1.9119	0.0000	-0.0655	-1.9087	0.0000
Si	-1.2958	1.3841	0.0000	-1.2831	1.3894	0.0000	-1.2874	1.3956	0.0000
Cl	3.0944	-2.5143	0.0000	3.1149	-2.5389	0.0000	3.1147	-2.5532	0.0000
Cl	-2.0535	-4.4380	0.0000	-2.0848	-4.4314	0.0000	-2.0858	-4.4445	0.0000
Cl	0.0091	3.2500	3.1438	0.0087	3.2574	3.1549	0.0117	3.2680	3.1581
Cl	0.0091	3.2500	-3.1438	0.0087	3.2574	-3.1549	0.0117	3.2680	-3.1581

^{1}**1**	MP2/cc-pVTZ			CCSD/cc-pVTZ			CCSD(T)/cc-pVTZ		
	x	y	z	x	y	z	x	y	z
C	-0.0961	-0.6485	0.0000	-0.0965	-0.6544	0.0000	-0.0956	-0.6498	0.0000
Si	-0.7800	4.9315	0.0000	-0.7657	4.9776	0.0000	-0.7703	4.9724	0.0000
Cl	-2.3176	2.1848	0.0000	-2.3067	2.2013	0.0000	-2.3345	2.1938	0.0000
Cl	3.6979	0.0538	0.0000	3.7080	0.0216	0.0000	3.7137	0.0340	0.0000
Cl	-1.0229	-2.6081	3.1760	-1.0367	-2.6155	3.1796	-1.0329	-2.6197	3.1839
Cl	-1.0229	-2.6081	-3.1760	-1.0367	-2.6155	-3.1796	-1.0329	-2.6197	-3.1839

^{2}**1**	MP2/cc-pVTZ			CCSD/cc-pVTZ			CCSD(T)/cc-pVTZ		
	x	y	z	x	y	z	x	y	Z
C	0.0000	2.7790	-3.6224	0.0000	0.0000	-1.8973	0.0000	0.0000	-1.9064
Si	0.0000	-2.7790	-3.6224	0.0000	0.0000	1.3348	0.0000	0.0000	1.3447
Cl	0.0000	0.0000	-1.9076	0.0000	2.7830	-3.6340	0.0000	2.7914	-3.6393
Cl	0.0000	0.0000	1.3408	0.0000	-2.7830	-3.6340	0.0000	-2.7914	-3.6393
Cl	0.0000	3.1961	3.4134	0.0000	-3.1892	3.4256	0.0000	-3.2037	3.4285
Cl	0.0000	-3.1961	3.4134	0.0000	3.1892	3.4256	0.0000	3.2037	3.4285

^{3}**1→2**	MP2/cc-pVTZ			^{1}**1→2**	MP2/cc-pVTZ		
	x	y	z		*x*	y	z
C	0.9591	-1.0084	0.0000	Cl	4.6016	-1.4325	-0.9600
Cl	1.3293	5.2913	0.0000	C	2.0678	0.6390	-1.1928
Cl	0.4819	2.3135	0.0000	Cl	-2.4189	-3.5427	1.0324
Si	-3.3453	0.9734	0.0000	Si	-1.0115	-0.2059	-0.2379
Cl	0.5416	-3.1259	3.1938	Cl	1.8728	2.8939	1.6564
Cl	0.5416	-3.1259	-3.1938	Cl	-3.9558	2.0268	-1.1292

Table 3.15: Symmetry-adapted internal coordinates for each stationary point used in vibrational analysis.

Triplet Silylcarbene (^{3}**1**)	Triplet Silylethylene (^{3}**2**)
$S_1 = r(1,2)$	$S_1 = r(1,2)$
$S_2 = r(1,3)$	$S_2 = 2^{-1/2}\,[r(1,3) + r(1,4)]$
$S_3 = 3^{-1/2}\,[r(2,4) + r(2,5) + r(2,6)]$	$S_3 = 2^{-1/2}\,[r(1,3) - r(1,4)]$
$S_4 = 6^{-1/2}\,[2r(2,4) - r(2,5) - r(2,6)]$	$S_4 = 2^{-1/2}\,[r(2,5) + r(2,6)]$
$S_5 = \theta(2,1,3)$	$S_5 = \theta(4,1,3)$
$S_6 = 6^{-1/2}\,[2\theta(1,2,4) - \theta(1,2,5) - \theta(1,2,6)]$	$S_6 = \theta(5,2,6)$
$S_7 = 3^{-1/2}\,[\theta(5,2,6) + \theta(4,2,5) + \theta(4,2,6)]$	$S_7 = 2^{-1/2}\,[\theta(2,1,3) - \theta(2,1,4)]$
$S_8 = 6^{-1/2}\,[2\theta(5,2,6) - \theta(4,2,5) - \theta(4,2,6)]$	$S_8 = \gamma(1,2,5,6)$
$S_9 = 2^{-1/2}\,[r(2,5) - r(2,6)]$	$S_9 = 2^{-1/2}\,[r(2,5) - r(2,6)]$
$S_{10} = 2^{-1/2}\,[\theta(1,2,5) - \theta(1,2,6)]$	$S_{10} = 2^{-1/2}\,[\theta(1,2,5) - \theta(1,2,6)]$
$S_{11} = 2^{-1/2}\,[\theta(4,2,5) - \theta(4,2,6)]$	$S_{11} = \gamma(2,1,3,4)$
$S_{12} = 3^{-1/2}\,[\tau(3,1,2,4) + \tau(3,1,2,5) + \tau(3,1,2,6)]$	$S_{12} = 2^{-1}\,[\tau(3,1,2,5) + \tau(3,1,2,6) + \tau(4,1,2,5) + \tau(4,1,2,6)]$

Singlet Silylcarbene (^{1}**1**)	Singlet Silylethylene (^{1}**2**)
$S_1 = r(1,2)$	$S_1 = r(1,2)$
$S_2 = r(1,3)$	$S_2 = 2^{-1/2}\,[r(1,3) + r(1,3)]$
$S_3 = 3^{-1/2}\,[r(2,4) + r(2,5) + r(2,6)]$	$S_3 = 2^{-1/2}\,[r(2,5) + r(2,6)]$
$S_4 = 6^{-1/2}\,[2r(2,4) - r(2,5) - r(2,6)]$	$S_4 = \theta(3,1,4)$
$S_5 = \theta(2,1,3)$	$S_5 = \theta(5,2,6)$
$S_6 = 6^{-1/2}\,[2\theta(1,2,4) - \theta(1,2,5) - \theta(1,2,6)]$	$S_6 = 2^{-1}\,[\tau(5,2,1,3) + \tau(6,2,1,3) + \tau(5,2,1,4) + \tau(6,2,1,4)]$
$S_7 = 3^{-1/2}\,[\theta(5,2,6) + \theta(4,2,5) + \theta(4,2,6)]$	$S_7 = \gamma(1,2,5,6)$
$S_8 = 6^{-1/2}\,[2\theta(5,2,6) - \theta(4,2,5) - \theta(4,2,6)]$	$S_8 = \gamma(2,1,3,4)$
$S_9 = 2^{-1/2}\,[r(2,5) - r(2,6)]$	$S_9 = 2^{-1/2}\,[r(1,3) - r(1,3)]$
$S_{10} = 2^{-1/2}\,[\theta(1,2,5) - \theta(1,2,6)]$	$S_{10} = 2^{-1/2}\,[r(2,5) - r(2,6)]$
$S_{11} = 2^{-1/2}\,[\theta(4,2,5) - \theta(4,2,6)]$	$S_{11} = 2^{-1/2}\,[\theta(2,1,3) - \theta(2,1,4)]$
$S_{12} = 3^{-1/2}\,[\tau(3,1,2,4) + \tau(3,1,2,5) + \tau(3,1,2,6)]$	$S_{12} = 2^{-1/2}\,[\theta(1,2,5) - \theta(1,2,6)]$

Triplet Transition State (^{3}**1**→**2**)
$S_1 = r(1,2)$
$S_2 = r(1,3)$
$S_3 = 2^{-1/2}\,[r(1,4) - r(2,4)]$
$S_4 = 2^{-1/2}\,[r(2,5) + r(2,6)]$
$S_5 = 2^{-1/2}\,[r(2,5) - r(2,6)]$
$S_6 = \theta(2,1,3)$
$S_7 = \theta(2,4,1)$
$S_8 = \theta(5,2,6)$
$S_9 = 2^{-1/2}\,[\theta(1,2,5) - \theta(1,2,6)]$
$S_{10} = \gamma(3,1,4,2)$
$S_{11} = 2^{-1/2}\,[\tau(5,2,4,1) + \tau(6,2,4,1)]$
$S_{12} = 2^{-1/2}\,[\tau(5,2,4,1) - \tau(6,2,4,1)]$

Table 3.16: Single-point energies for each stationary point at the MP2/cc-pVTZ reference geometry.

1 (^{3}A″)

	ROHF	ROZAPT2	ROCCSD	ROCCSD(T)
cc-pVTZ	-2164.983612	-2165.945280	-2166.019206	-2166.065991
cc-pVQZ	-2165.007520	-2166.065086	-2166.133008	-2166.188943
cc-pV5Z	-2165.015171	-2166.114215	-2166.172158	

2 (^{3}A″)

	ROHF	ROZAPT2	ROCCSD	ROCCSD(T)
cc-pVTZ	-2164.927960	-2165.906880	-2165.975548	-2166.024622
cc-pVQZ	-2164.951220	-2166.025672	-2166.087790	-2166.146116
cc-pV5Z	-2164.958305	-2166.073941	-2166.126009	

2 (^{1}A$_1$)

	RHF	RMP2	RCCSD	RCCSD(T)
cc-pVTZ	-2164.921946	-2165.941513	-2165.998382	-2166.051710
cc-pVQZ	-2164.945924	-2166.062461	-2166.111978	-2166.174669
cc-pV5Z	-2164.953482	-2166.111563	-2166.150682	

1 (^{1}A′)

	RHF	RMP2	RCCSD	RCCSD(T)
cc-pVTZ	-2164.946452	-2165.935101	-2166.004297	-2166.054794
cc-pVQZ	-2164.970253	-2166.056423	-2166.118635	-2166.178437
cc-pV5Z	-2164.977778	-2166.106092	-2166.157890	

2 → **1** (^{3}A″)

	RHF	RMP2	RCCSD	RCCSD(T)
cc-pVTZ	-2164.850263	-2165.844357	-2165.912522	-2165.966930
cc-pVQZ	-2164.873868	-2165.963469	-2166.024843	-2166.088756
cc-pV5Z	-2164.881170	-2166.011965	-2166.063230	

2 → **1** (^{1}A)

	RHF	ROZAPT2	RCCSD	RCCSD(T)
cc-pVTZ	-2164.875874	-2165.895626	-2165.952826	-2166.007649
cc-pVQZ	-2164.899720	-2166.017194	-2166.066789	-2166.131156
cc-pV5Z	-2164.907252	-2166.066805	-2166.105876	

Table 3.17: Internal coordinate quadratic force field for several stationary points using the internal coordinates defined in Table 3.15.

Triplet silylcarbene (^{3}**1**)

	1	2	3	4	5	6	7	8
1	4.7301							
2	-0.2082	3.5422						
3	0.1208	0.2053	3.5350					
4	-0.0154	0.0123	0.0603	3.1233				
5	0.2557	0.2197	0.0041	0.0335	0.2835			
6	0.0920	0.0680	0.0157	0.2479	0.0801	0.6571		
7	-0.1393	-0.2542	0.2368	-0.0130	0.0214	-0.0169	1.7653	
8	-0.0316	-0.0252	0.0098	-0.2405	-0.0368	-0.1422	0.0293	0.7674

	9	10	11	12
9	3.0260			
10	0.2307	0.5923		
11	0.2265	0.1404	0.7389	
12	-0.0009	-0.0112	0.0141	0.0050

Triplet silylethylene (^{3}**2**)

	1	2	3	4	5	6	7	8
1	3.1006							
2	0.0550	4.5202						
3	0.0054	-0.0442	3.4779					
4	0.1405	0.1108	0.0245	3.0962				
5	-0.1236	0.3494	0.0246	-0.0600	1.2775			
6	-0.0459	-0.0436	-0.0152	0.1549	0.0100	0.8388		
7	0.0102	-0.0220	0.3273	-0.0333	0.0144	0.0037	0.3923	
8	0.1033	0.0085	-0.1209	0.0891	-0.0073	-0.0128	-0.0783	0.6186

	9	10	11	12
9	2.7644			
10	0.1378	0.5201		
11	0.0053	0.0124	0.1136	
12	0.0317	0.0218	-0.0288	0.0112

Singlet silylcarbene (^{1}**1**)

	1	2	3	4	5	6	7	8
1	2.5917							
2	-0.0788	4.4972						
3	0.0414	0.1106	3.4700					
4	0.0263	-0.0083	-0.0744	3.0172				
5	0.3863	0.5419	0.0357	-0.1144	0.8716			
6	0.0984	-0.2281	-0.0352	0.2194	-0.0823	0.5990		
7	-0.1223	-0.1088	0.2362	0.0367	-0.0992	-0.0420	1.7674	
8	0.0638	0.0444	-0.0109	-0.195	0.0308	-0.1155	-0.0530	0.6893

	9	10	11	12
9	3.0902			
10	0.1888	0.4128		
11	0.2088	0.0764	0.7304	
12	0.0080	-0.0460	0.0061	0.0107

Singlet silylethylene (^{1}**2**)

	1	2	3	4	5
1	5.3148				
2	0.3315	4.2837			
3	-0.0060	0.1176	3.5936		
4	-0.1935	0.2041	-0.0504	1.2435	
5	-0.1543	-0.0052	0.1300	0.0596	0.8096

	6
6	0.0771

	7	8
7	0.1013	
8	0.1403	0.2565

	9	10	11	12
9	3.5048			
10	0.0137	3.3803		
11	0.4506	0.0742	0.4690	
12	0.1141	0.1843	0.0275	0.4965

CHAPTER 4

CONCLUSIONS

The *ab initio* methods applied to these two systems are at the fore-front of accurate methods that can currently be applied to reasonably sized systems. The methods MP2, CCSD, and CCSD(T) are fairly well tested by this point and can be trusted to provide results that are consistent and accurate for most systems without a great amount of multi-reference character. The newer methods that apply triples contributions iteratively, CCSDT-3 and CC3 also appear to do fairly well, especially with respect to their perturbative analog CCSD(T). The EOM method also appears to perform quite well in excited state calculations. These methods prove themselves to be powerful tools in the prediction of experimental properties and as aids to the determination of experimentally derived conclusions.